NAVAL POSTGRADUATE SCHOOL

MONTEREY, CALIFORNIA

THESIS

NEW BOTTOM ROUGHNESS CALCULATION FROM MULTIBEAM ECHO SOUNDERS FOR MINE WARFARE

by

Patrick J. Earls

September 2012

Thesis Advisor:	Peter Chu
Second Reader:	Ronald Betsch

Approved for public release; distribution is unlimited

THIS PAGE INTENTIONALLY LEFT BLANK

REPORT DOCUMENTATION PAGE			Form Approved OMB No. 0704-0188
Public reporting burden for this collection of information is estimated to average 1 hour per response, including the time for reviewing instruction, searching existing data sources, gathering and maintaining the data needed, and completing and reviewing the collection of information. Send comments regarding this burden estimate or any other aspect of this collection of information, including suggestions for reducing this burden, to Washington headquarters Services, Directorate for Information Operations and Reports, 1215 Jefferson Davis Highway, Suite 1204, Arlington, VA 22202-4302, and to the Office of Management and Budget, Paperwork Reduction Project (0704-0188) Washington DC 20503.			
1. AGENCY USE ONLY *(Leave blank)*	**2. REPORT DATE** September 2012	**3. REPORT TYPE AND DATES COVERED** Master's Thesis	
4. TITLE AND SUBTITLE New Bottom Roughness Calculation from Multibeam Echo Sounders for Mine Warfare		**5. FUNDING NUMBERS** N6230611PO00123 N0001412WX20510	
6. AUTHOR(S) Patrick J. Earls			
7. PERFORMING ORGANIZATION NAME(S) AND ADDRESS(ES) Naval Postgraduate School Monterey, CA 93943-5000		**8. PERFORMING ORGANIZATION REPORT NUMBER**	
9. SPONSORING /MONITORING AGENCY NAME(S) AND ADDRESS(ES) Naval Oceanographic Office, 1002 Balch Blvd Stennis Space Center, MS 39529; Office of Naval Research/CRUSER		**10. SPONSORING/MONITORING AGENCY REPORT NUMBER**	
11. SUPPLEMENTARY NOTES The views expressed in this thesis are those of the author and do not reflect the official policy or position of the Department of Defense or the U.S. Government. I.R.B. Protocol number N/A.			
12a. DISTRIBUTION / AVAILABILITY STATEMENT Approved for public release: distribution is unlimited		**12b. DISTRIBUTION CODE**	

13. ABSTRACT (maximum 200 words)

Bottom roughness has a significant effect on acoustic backscattering on the ocean bottom. Sonar systems rely on backscattering and shadows for detecting objects lying on the seafloor. The seafloor is rather complex including craters, gullies, seaweed, rocks, sand ridges, tall obstructions, deep holes and sloping regions. Underwater mines can be hidden around these objects to make detection more difficult. High resolution (1 m × 1 m) seafloor data collected by the Navy using multibeam echo sounder (EM710) off the western coast of Saipan was processed by the MB Systems. The advanced least-square method is used to establish new bottom reference level from the EM710 data. After removing the reference level, the high-resolution bathymetry data converts into bottom roughness percentage using a threshold. The calculated bottom roughness percentage is ready to be incorporated into the current Navy doctrine. Two new (gradient and mathematical morphology) methods have been developed in this thesis to calculate the bottom roughness without the reference level. Statistical analysis was conducted to illustrate the added value of the new bottom roughness calculation.

14. SUBJECT TERMS Mine Warfare, Bottom Roughness, EM710 Multibeam Echo Sounder, Bathymetry, Backscattering.			**15. NUMBER OF PAGES** 80
			16. PRICE CODE
17. SECURITY CLASSIFICATION OF REPORT Unclassified	**18. SECURITY CLASSIFICATION OF THIS PAGE** Unclassified	**19. SECURITY CLASSIFICATION OF ABSTRACT** Unclassified	**20. LIMITATION OF ABSTRACT** UU

NSN 7540-01-280-5500 Standard Form 298 (Rev. 2-89)
Prescribed by ANSI Std. 239-18

THIS PAGE INTENTIONALLY LEFT BLANK

Approved for public release; distribution is unlimited

NEW BOTTOM ROUGHNESS CALCULATION FROM MULTIBEAM ECHO SOUNDERS FOR MINE WARFARE

Patrick J. Earls
Lieutenant, United States Navy
B.S., Maine Maritime Academy, 2006

Submitted in partial fulfillment of the
requirements for the degree of

MASTER OF SCIENCE IN PHYSICAL OCEANOGRAPHY

from the

NAVAL POSTGRADUATE SCHOOL
September 2012

Author: Patrick J. Earls

Approved by: Peter C. Chu
Thesis Advisor

Ronald E. Betsch (NAVO)
Second Reader

Mary L. Batteen
Chair, Department of Oceanography

THIS PAGE INTENTIONALLY LEFT BLANK

ABSTRACT

Bottom roughness has a significant effect on acoustic backscattering on the ocean bottom. Sonar systems rely on backscattering and shadows for detecting objects lying on the seafloor. The seafloor is rather complex including craters, gullies, seaweed, rocks, sand ridges, tall obstructions, deep holes and sloping regions. Underwater mines can be hidden around these objects to make detection more difficult. High resolution (1 m × 1 m) seafloor data collected by the Navy using multibeam echo sounder (EM710) off the western coast of Saipan was processed by the MB Systems. The advanced least-square method is used to establish new bottom reference level from the EM710 data. After removing the reference level, the high-resolution bathymetry data converts into bottom roughness percentage using a threshold. The calculated bottom roughness percentage is ready to be incorporated into the current Navy doctrine. Two new (gradient and mathematical morphology) methods have been developed in this thesis to calculate the bottom roughness without the reference level. Statistical analysis was conducted to illustrate the added value of the new bottom roughness calculation.

THIS PAGE INTENTIONALLY LEFT BLANK

TABLE OF CONTENTS

LIST OF FIGURES

LIST OF TABLES

THIS PAGE INTENTIONALLY LEFT BLANK

I. INTRODUCTION

A. MINE WARFARE

Mine warfare (MIW) consists of offensive mining, defensive mining, and mine countermeasures (MCM). Offensive mining is the laying of mine fields to actively seek out and sink enemy vessels. Defensive mining is the process of using mine fields to block enemy ships from entering critical waters. Mine countermeasures is seeking out and removing mine fields or neutralizing them.

Naval mines are self-contained explosive devices that are left behind and used to detonate and damage enemy submarines and surface ships. Mines are an effective way to engage in warfare on the cheap. Most mines are relatively inexpensive compared to building/purchasing warships, their easy to manufacture, and have long on station times. This makes them very attractive to belligerents who like to fight in asymmetric warfare. This means state and non-state players alike can engage in mine warfare (MIW) anywhere around the world at any time. The key objective of a naval mine is to sink enemy ships. Mines are indiscriminate when comes to choosing enemies and can attack even a friendly ship if it gets to close. Unlike other conventional naval weapons, mines are laid in ocean and wait for prolonged periods for a ship to sail by and trigger the activation mechanism. Mines can also be laid in groups of patterns to ensure the probability of their success.

Multiple platforms can act as a delivery device for laying mines. These platforms include surface ships, submarines, and aircraft. Surface ships throughout history have been the work horse for laying mines. Their weight capacity, allows for a large number of mines to be delivery, unlike submarines and aircraft who both have limited space. Submarines are a tool of stealth can concealment, which makes them ideal for delivery mines that are hidden to you enemy. The negative to surface ships and submarines, is the time to get on station and the fear that their in the water with mines that could accidently detonate at any moment. Aircraft are an effective delivery device because they can

quickly get on station anywhere you want to setup a mine field and are not at the same risk as the delivery platforms in the water. Laying mines is a lot easier than recovering mines.

Figure 1. B-52 Dropping Quickstrike Mines (From Brissette 1997)

There are several types of mines in the world today, and they are classified based off several factors. The first factor is the method of detonation. The earliest mines were called contact mines and are still used today, because of their simplicity and low cost. Contact mines have quite a simple triggering device. They detonate as they contact an enemy vessel. As technology advanced through time, new and more effective ways of triggering mines have been created: Magnetic sensors, acoustic, water pressure, and electronic/remote controlled fuses. Ships are made of steel and carry large electric equipment that creates a large magnetic signature. Magnetic sensors use magnetometers to detect changes in the magnitude field surrounding the area. Figure 2 shows the

different permanent and electrical influence fields of a surface ship. Acoustic sensors use passive sonar to detect the acoustic signature of a ship. The common acoustic sources for a ship are seen in Figure 3.

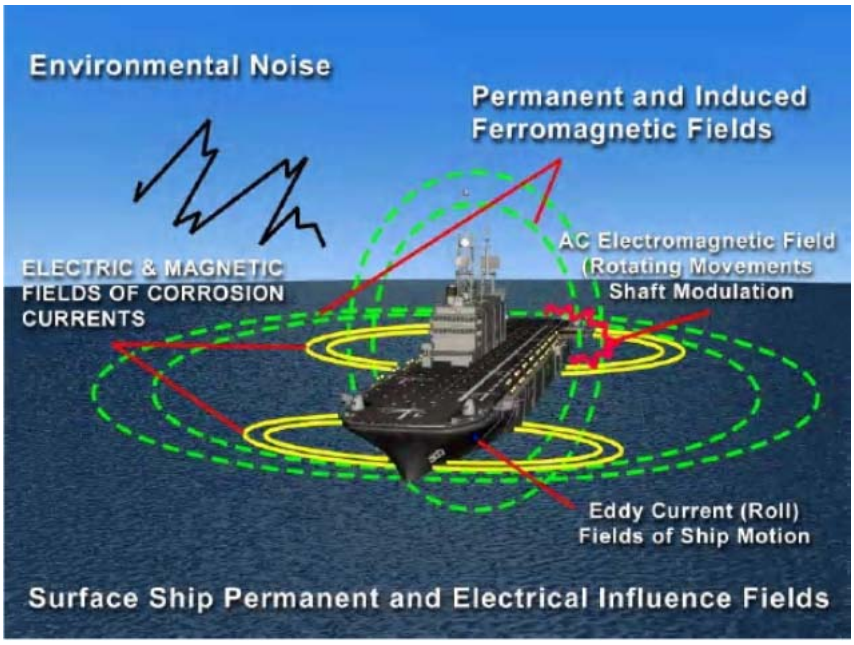

Figure 2. Surface ship magnetic and electrical influence field (From NSWC 2007)

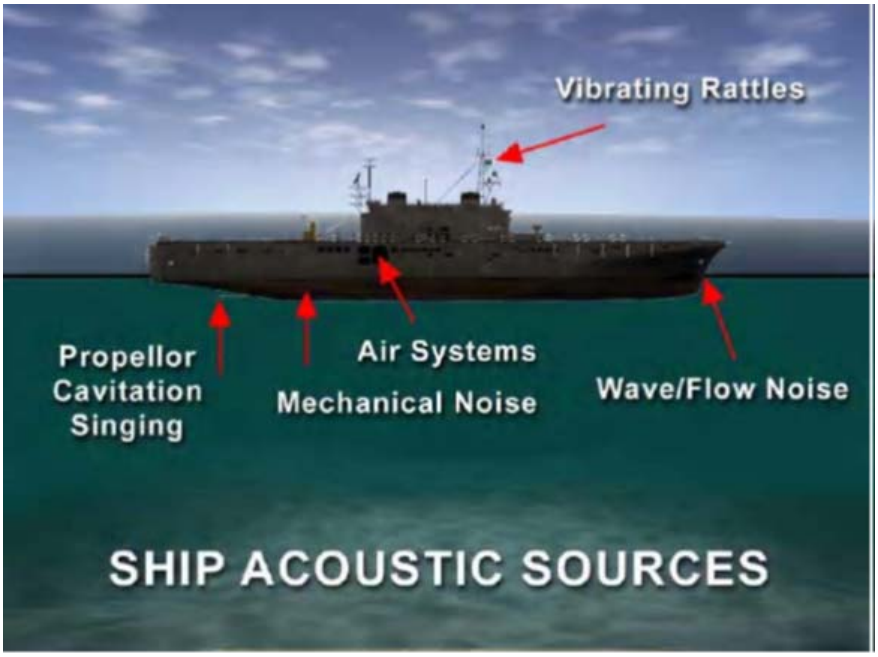

Figure 3. Common ship acoustic noise sources (From NSWC 2007)

Pressure mines use the variation between high and low pressures relative to the normal pressure of the ocean that the displacement of a ship makes as it passes above the sensor. Figure 4 illustrates the ships pressure signature.

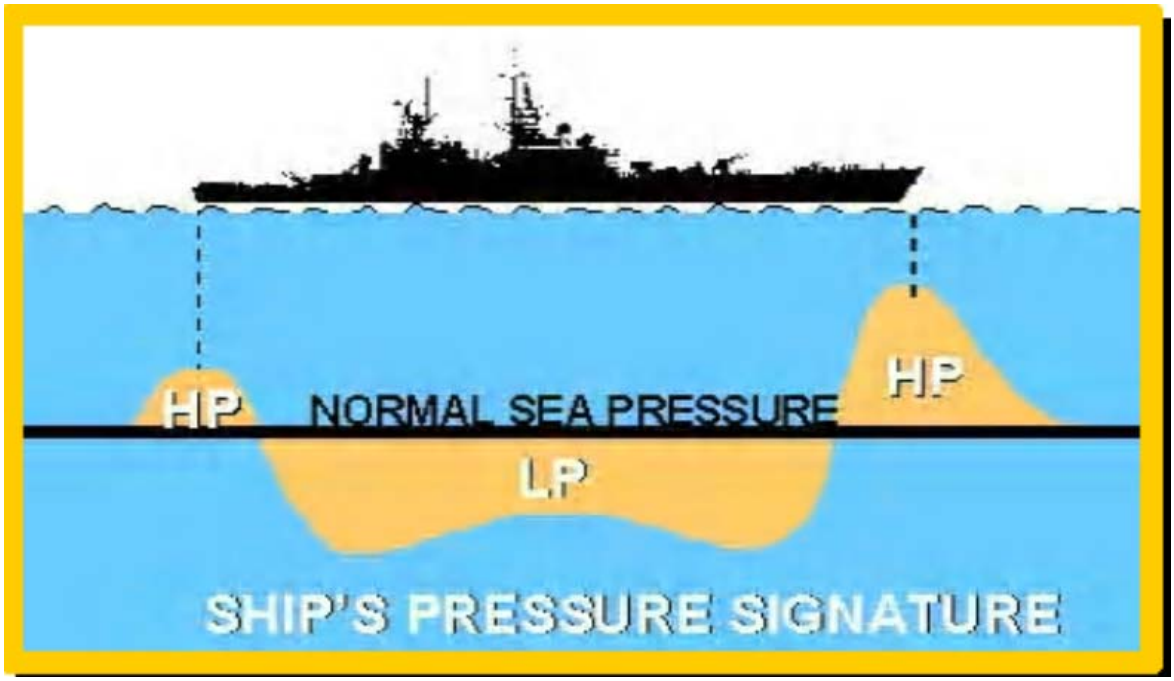

Figure 4. Ship's pressure signature (From NSWC 2007)

Electronic mines use a combination of sensors, including magnetic and acoustic to help detect a vessel and satisfy the mines firing logic. Modern acoustic sensors look for a unique acoustic signature of a certain ship, preventing them from attacking anything else. Firing logic determines when the mine should actuate and ranges from very simple (signal rate and amplitude) to highly sophisticated (microprocessors that algorithmically analyze multiple signals to be more discriminating and minimize non-target actuations) (NSWC 2007). Figure 5 depicts the mine actuation process from start to finish.

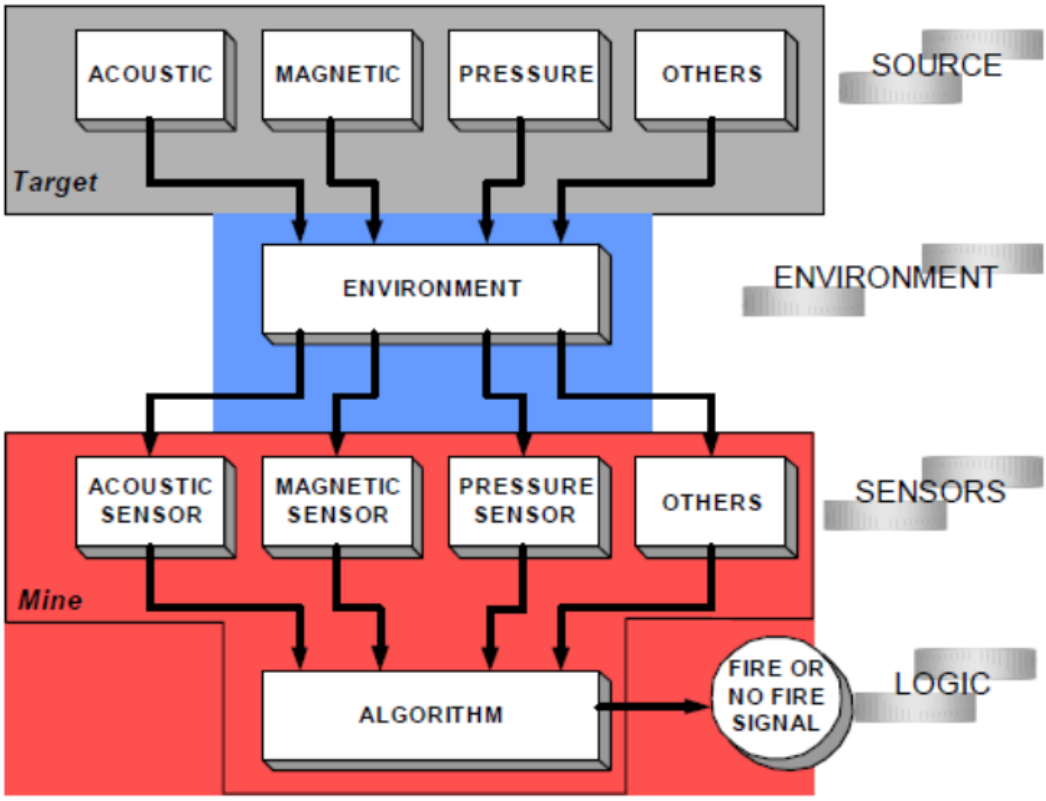

Figure 5. Source signatures to mine actuation process (From NSWC 2007)

Another way the mines are classified is by their position in the water column. There are three categories of positions for mines: moored mines, moving mines, and bottom mines. Certain mines can be set to float in the water and be attached to a steel cable that is connected to an anchor; these are called moored mines or floating. This allows the mine to float at different depths, depending on the type of ship you are trying to sink. The mine could sit at a depth that only comes into contact with ships with deeper drafts and avoid small ships. Another type of moored mine is a volume mine which is a mine of positive buoyancy that is located within the water column. Moored mines can be used in both the deep water and the shallow water arena. The objective in shallow waters is to be mindful of tides and understand how they might affect the mine during a low tide period. The second category of mines is a type of mine that drifts instead of being moored, which makes them harder to predict. These are called moving mines and are more trouble than their worth. Ocean currents can move these mines in various directions

making it more challenging to keep track them and also for removal later on. The third category of mine and the most difficult to detect is a bottom mine. These are mines that lay on the ocean seafloor and wait for a vessel over top to sail by. Because these mines lay on the ocean bottom, mine countermeasure ships have difficulty detecting/locating them, due to terrain features, surface sediment, and roughness. Mines can also be buried along the seafloor to prevent detection. Figure 6 shows a diagram of mines locations in the ocean. Defeating this threat requires an understanding of the ocean environment, along with the resources and technology available to render the threat inactive.

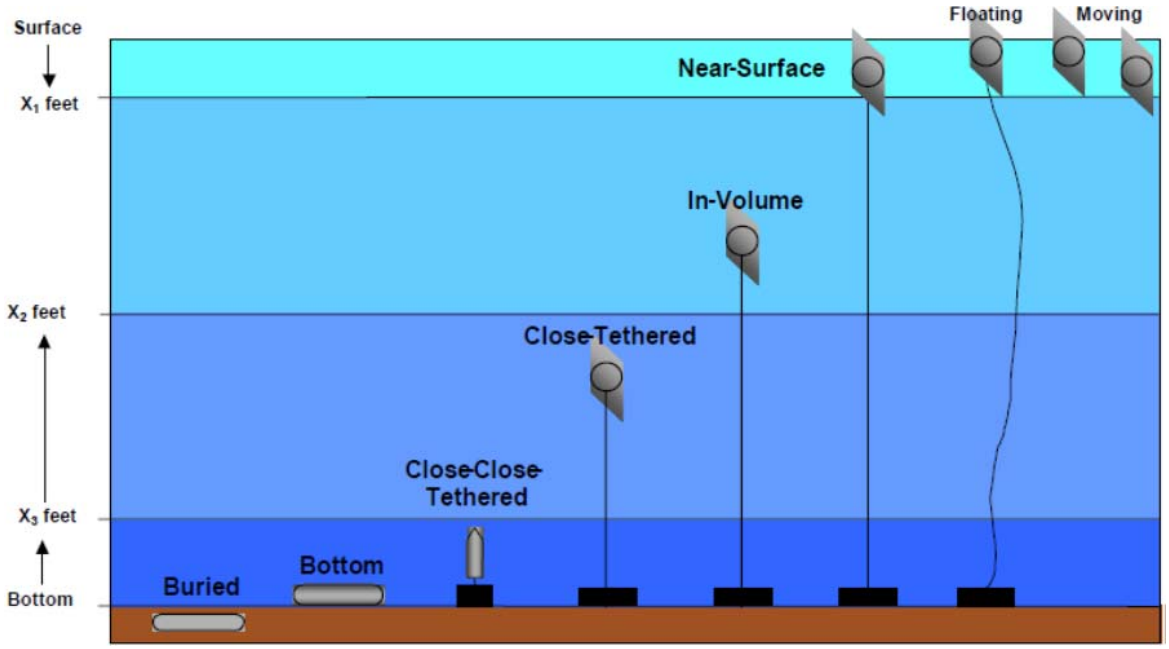

Figure 6. Mine locations in the ocean (From NSWC 2007)

B. CURRENT BOTTOM ROUGHNESS DETERMINATION

The definition of roughness is the measure of the ridge height along the ocean bottom. Doctrine from the U.S. Navy (NWP 3-15) defines roughness as craters, gullies, seaweed, sand ridges, tall obstructions, deep holes, or steeply sloping regions. Slopes can make it possible for mines to move to new locations. Rocks and holes on the seafloor help mines remain hidden or camouflage from MCM sensors. All the obstructions and obstacles are considered roughness under the doctrine. The effects of the bottom seafloor

texture on detecting mines are called roughness parameters. The U.S. Navy doctrine separates the bottom roughness parameters into three categories which follow under the bottom profile group. The three categories are smooth, moderate, and rough. The U.S. Navy current doctrine for roughness analysis is shown in Table 1. Previous studies showing the importance of bottom roughness can be seen in statistical features of sea-floor (Bell 1975). Other works include statistical characterization of seafloor roughness (Berkson and Matthews 1984) and quantitative methods for analyzing the roughness of the seafloor (Fox and Hayes 1985).

For non-sand ridge, the bottom roughness percentage is used. It is represented by the ratio of the area containing craters, gullies, and rocks versus the overall area. Knowledge of the location and the size of the roughness are required to calculate the bottom roughness percentage and are usually difficult to determine. Unfortunately, the bottom roughness percentage is too ambiguous for analysis. Once the percentage is calculated and the bottom profile group is determined, the detail of the roughness is still unknown. The only thing known is a vague and general idea of the terrain to be analyzed, nothing else. For sand ridge bottom, the sand ridge height is used to represent the bottom roughness. Before using the Navy doctrine, a reference level (or sometimes called mean bottom slope) needs to be determined.

Roughness Category	**Bottom Roughness Percentage**	**Sand Ridge Height (m/ft)**
Smooth	Less than 5	Less than 0.2/*0.3*
Moderate	5 to 15	0.2 to 0.3/*0.5 to 1.0*
Rough	Over 15	Over 0.3/*1.0*

Table 1. U.S. Navy current doctrine for roughness analysis (From NWP 3-15.2)

C. PURPOSE OF THIS THESIS

The purpose of this thesis is to provide a new method for determining the bottom roughness of the seafloor without requiring a reference level. The new method to determine roughness will be using gradient and mathematical morphology of a terrain. This research is important because bottom roughness has a significant effect on

backscattering on the seafloor. Sonar systems rely on backscatter and shadows in order to detect an object lying on the seafloor. If the object location is unknown, then ships are susceptible to attack from mine like objects. The seafloor can be rather complex; craters, gullies, seaweed, rocks, sand ridges, tall obstructions, deep holes and sloping regions are all forms of bottom roughness. Underwater mines can be hidden around these objects to make it more difficult for detection. A simple and effective algorithm has been developed in this thesis for effective determination of bottom roughness, which will contribute to mine detection and MCM operations. The high-resolution EM710 multibeam echo sounder data collected off the west coast of Saipan are used for illustration.

II. BACKGROUND

A. MULTIBEAM ECHO SOUNDERS

1. Sonar Equation and Backscattering Strength

The acoustic echoing process is made up of different parts and can be expressed in the sonar equation:

$$SN = SL - 2TL + BTS - NL + DI \quad (1)$$

In the equation, signal to noise ratio (SN) is the strength of the echo return. The amount of acoustic energy transmitted through the water is the source level (SL). The loss of the signal due to spherical spreading and absorption is called transmission loss (TL). It is multiplied by two, because the signal travels to the location and back. (NL) is the noise level and (DI) is the directivity index. The last part of the equation is the bottom target strength (BTS) or known as the backscattering strength. The BTS will be dependent on the reflective property of the seabed and also by the extent of the bottom area that contributes to the backscattered signal at the time (Hammerstad 2000). The backscatter strength is derived from the intensity of the returned signal from the seabed. From the sonar equation, an equation can be derived for the echo level (EL) of the signal backscattered from the bottom:

$$EL = SL - 2TL + BTS. \quad (2)$$

To solve for transmission loss:

$$2TL = 2\alpha R + 40 \log R; \quad (3)$$

where α is the absorption coefficient (in dB/m), and R is the range.

The backscattering area will be bounded by the beam geometry, that is defined asθ_x , andθ_y, at normal incidence (0° incidence angle or 90 degree grazing angle) while in other directions it will be bounded by the transmit pulse length, τ and by the along-track beamwidth, θ_x (Hammerstad, 2000)

$$BTS = BS + 10log\theta_x \theta_y R^2 \quad \text{for } \varphi = 0^\circ, \quad (4)$$

$$BTS = BS + 10log\frac{c\tau}{2sin\varphi}\theta_x R \quad for\ \varphi > \ 0^{\circ}. \tag{5}$$

where c is the speed of sound and φ is the angle of incidence.

2. Echo Sounders

Echo sounding is the process of transmitting acoustic pulses from the sea surface down to the seafloor and listening for the echo (reflection) to return. This process is used to measure the depth of the ocean. For bathymetric survey, the depth is measured at the point directly below the echo sounder of the vessel. A multibeam echo sounder is a system designed to map multiple locations of the seafloor with just a single ping, providing quicker surveys. The locations are arranged in a contiguous area of the seafloor, this area is known as the swath. The dimensions of the swath are called the swath width. The swath width is measured in the across track and the athwart ship directions. Figure 7 shows the swath of a multibeam sonar.

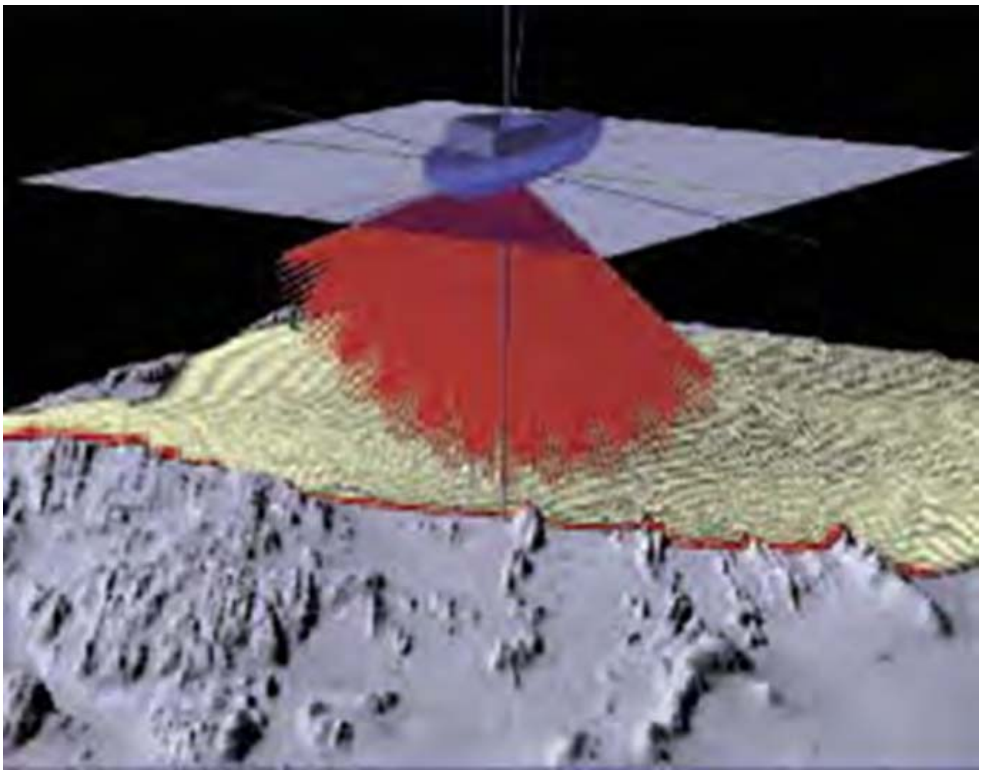

Figure 7. Multibeam echo sounder swath (From USGS 1998)

Multibeam echo sounder systems can provide two sources of data. They can provide bathymetry data and backscattering strength. Both sources of data are critical for mapping the seafloor and determining the roughness.

B. EM710

The system used to gather the bathymetry and backscattering data for this thesis was the Krongsberg Maritime EM710 multibeam echo sounder. The EM710 is a multibeam echo sounder that has the capability to map the ocean seafloor with high resolution.

Figure 8. EM710 multibeam echo sounder (From NOAA 2011)

This system is very effective in shallow waters and the minimum operating depth is roughly 3 meters below the transducer. For deeper water, the maximum operating depth is approximately 2000 meters. The optimal depth for survey ranges from 10 to 500 meters, due attenuation limitations at deeper depths. The EM710 sonar operating frequencies range from 70 to 100 kHz, with the capability to provide 6 sectors in dual swath mode (Kongsberg Maritime AS 2011). The swath width or the across track

coverage is 5.5 times the water depth. The EM710 provides 0.5 degree (min) high resolution data, which far surpasses older echo sounders. The ping rate setup on the EM710 is a special feature. Two sound speed profiles are generated for every ping cycle, this to ensure 100% coverage of the seafloor with high resolution data at high survey speeds. The EM710 offers different resolution and range levels, depending on the receiver beam widths. To ensure the highest resolution, beam focusing is applied to transmit and receive beams. The EM710 through the use of electronic stabilization of the transmitted beams and received beams can correct for roll, pitch, and yaw. Table 2 lists the technical specifications of the EM710 multibeam echo sounder.

Technical Specifications	
Operating frequency	70 – 100 kHz
Max ping rate	30 Hz
Swath coverage sector	Up to 140 deg
Minimum depth	3 meters below transducer
Maximum depth	2000 m
CW transmit pulses	0.2 to 2 ms
FW sweep pulse	Max 120 ms
System accuracy	Less than 2 cm
Maximum number of soundings per ping	800 (Dual Swath mode)
Max coverage	2400 m
Transducer choices	0.5 x 1 degree
Pulse form	CW & FM
Pulse width	25µs -12ms
TX dimensions (L x W x H)	1940 x 224 x 118 mm
RX dimensions (L x W x H)	970 x 224 x 118 mm

Table 2. EM710 technical specifications (From Kongsberg Maritime AS 2011)

III. RAW MULTIBEAM SONAR DATA PROCESS

The EM710 multibeam data off the west coast of Saipan was collected by the Naval Oceanographic Office (NAVOCEANO) and was in raw format. MB-systems software Caress et al. (2010) was used to process and display the raw data. Matlab was used to analyze bathymetry data as well as to determine the bottom roughness.

A. MB-SYSTEMS

1. Organizing and Surveying the Data

MB-Systems is a useful software tool for mapping the seafloor by processing multibeam bathymetry and backscatter imagery data. The first step is to organize the data by creating ancillary files. Each segment of data has a statistics, bathymetry, and navigation file attached to it. These ancillary data files are used by programs to process and plot the data inside MB-systems. A program called mbdatalist is used to organize the data into lists. After everything is organized, a quick a survey is conducted to get an idea of the lay of the sea floor and the quality of the data. Mbm_plot is a useful tool for plotting the bathymetry data.

The original survey was conducted over a large area and multiple ship track patterns. To select only a certain region to process, mbcopy was used remove the unwanted areas of data. A new updated survey area is now created to begin processing.

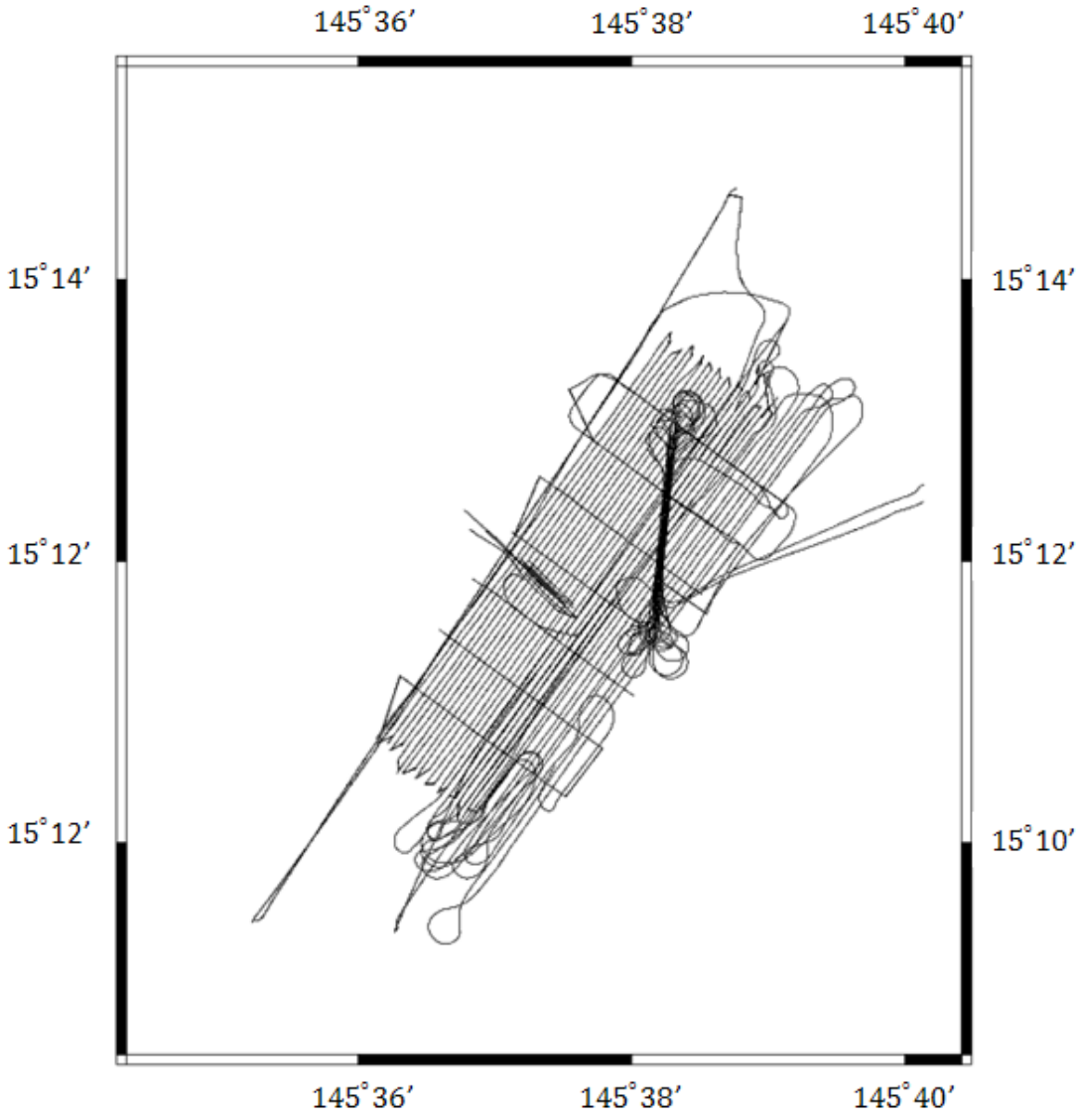

Figure 9. The original EM710 data range

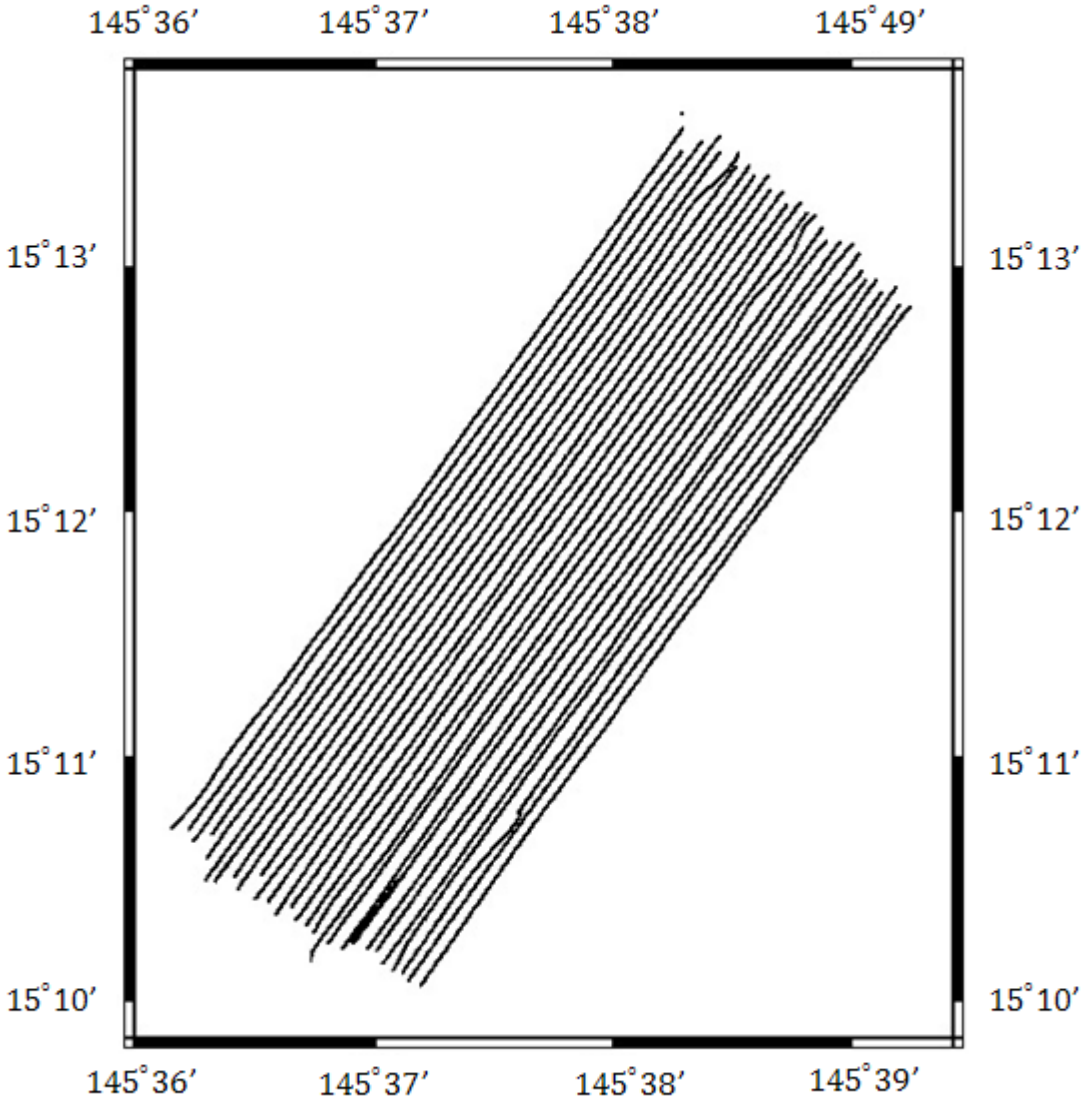

Figure 10. New updated survey area

2. Processing the Data

a. Pitch and Roll Bias

After the data is organized, it is time to start processing the data. The first step in processing the data is to determine the roll bias. As the ship conducts the survey at sea the multibeam sonar is continuously moving in respect to the ships motion. The data needs to be corrected for any bias introduced by the changing pitch and roll of the ship. "Roll bias is a measure of the difference between the atwartship alignment of the ship's multibeam hydrophone array, and that of its vertical reference source" (Caress et al. 2010). The roll and pitch bias values for each region of the survey are determined by using the mbrollbias and mbpitchbias programs. Two segment lines of the data are selected as input files into the mbrollbias. The program calculates the bias correction for that region and through mbset applies it to the entire data set.

b. Correcting the Sound Speed Profile

The next step is to determine the correct sound speed profile (SSP). High quality multibeam sonar data requires an accurate SSP. As discussed in chapter two, sound travel in the ocean can different effects on the data. MB-systems has programs like mbvelocity tool and mblevitus for calculating a new SSP. Multiple sources of data can help determine the correct SSP. Historical temperature, salinity, and pressure data can be a useful source. MbLevitus provides a historical database for which it creates a SSP. During the survey, accurate sound speeds and depths were inputted into the EM710 data through direct measurements. Using mbvelocity tool the direct measurement and mblevitus historical SSP's were loaded and manipulated in real time; a new SSP was created for the data set.

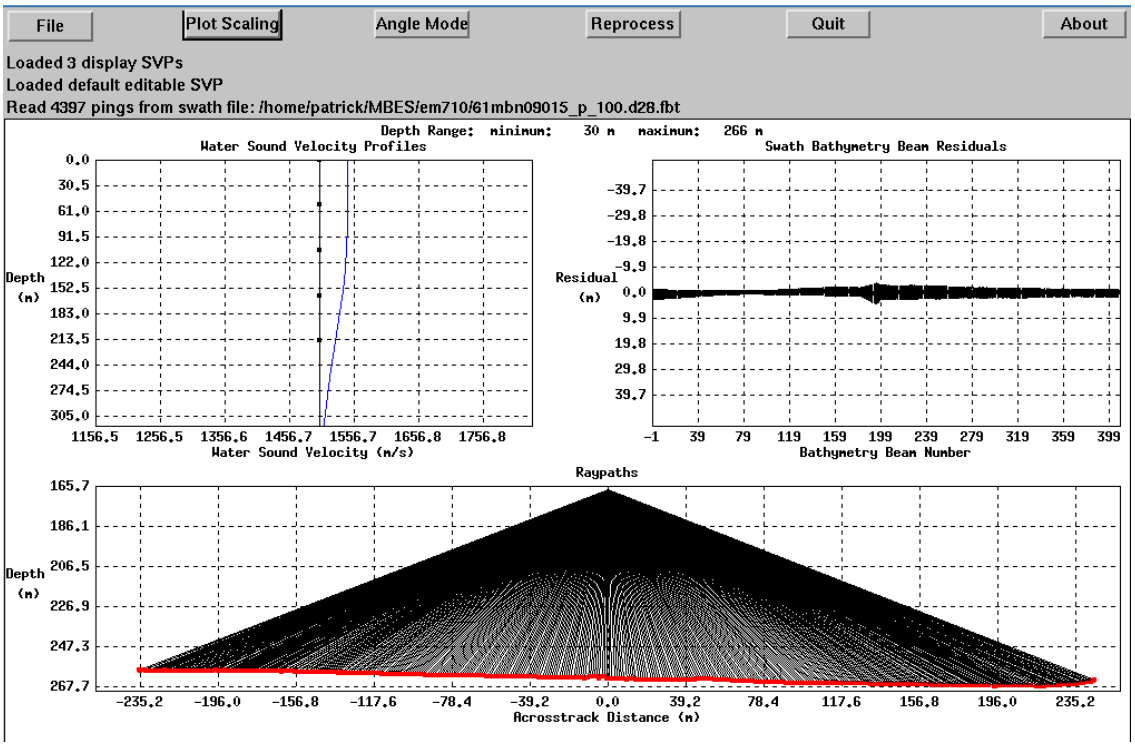

Figure 11. MB-systems mbvelocity tool

c. Cleaning the Navigation Data

Electronic navigation systems are used to input accurate position information to the EM710 multibeam sonar. Data collected by the EM710 is only as good as the navigation data received. The global positioning system (GPS) unit is the most common electronic navigation system. Navigation systems are not perfect and from time to time have various kinds of errors. MB-systems has an interactive tool called mbnavedit that allows you to assess the quality of navigation data inputted into the multibeam sonar and edit it as seen in Figures 12 and 13.

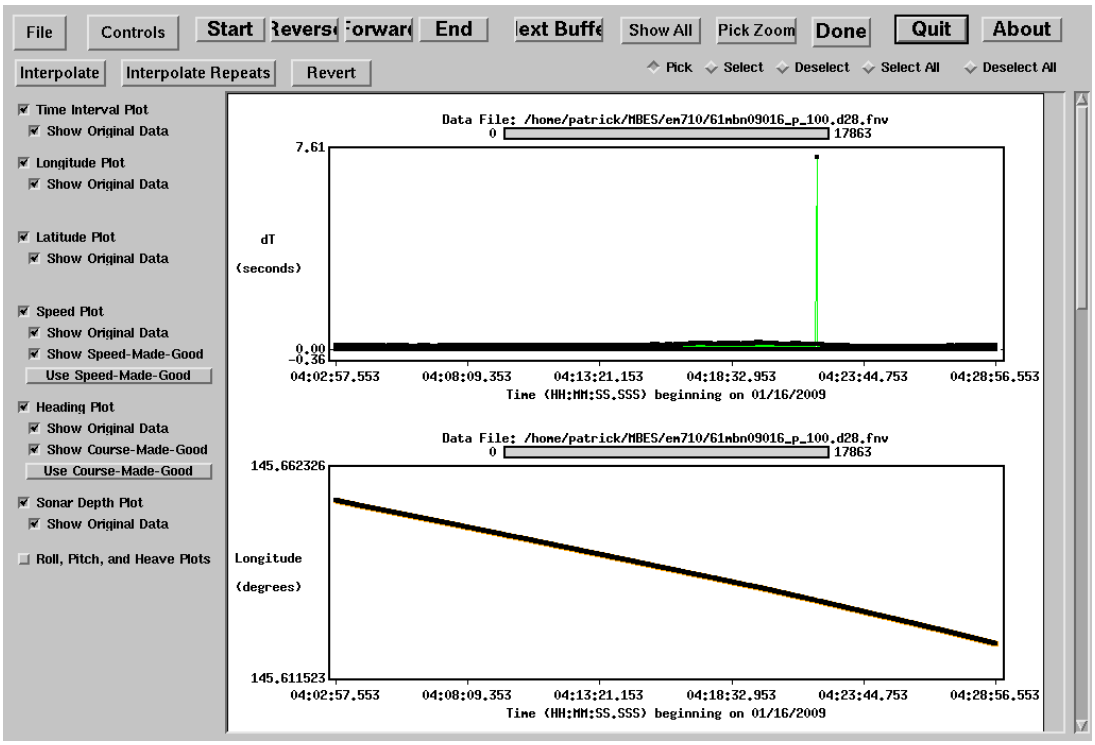

Figure 12. MB-systems mbnavedit tool

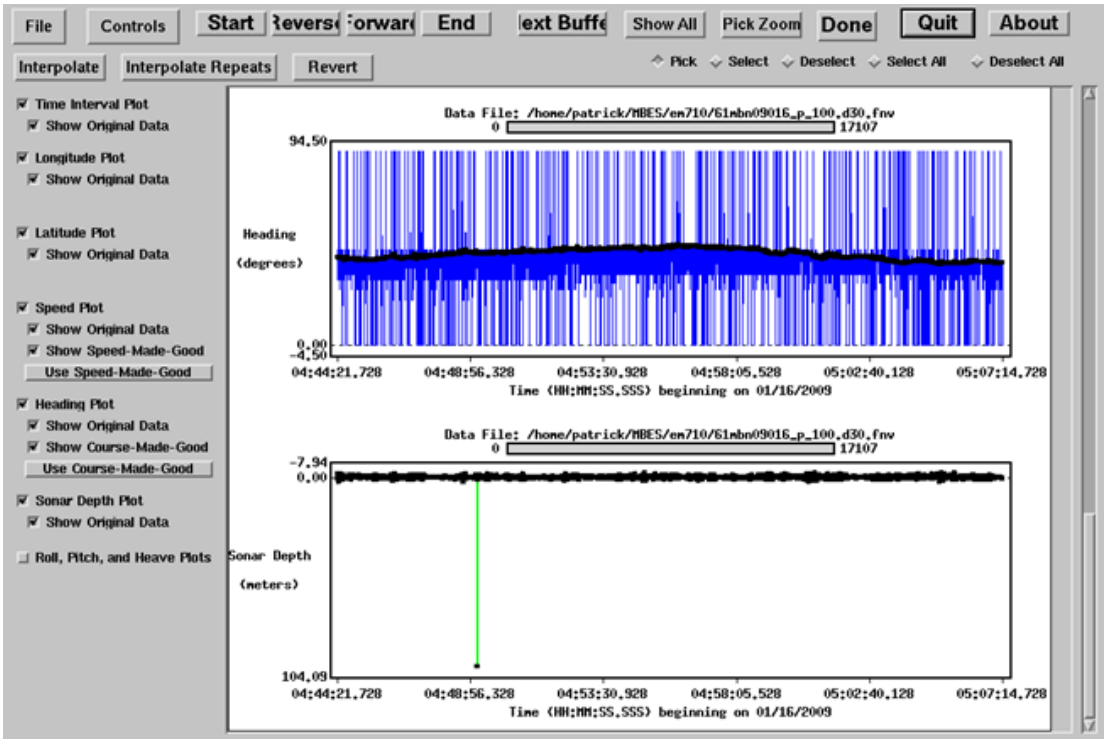

Figure 13. MB-systems mbnavedit tool continued

d. Flagging Bathymetry Data

Now it is time to edit the bathymetry data by flagging erroneous data points. Errors in multibeam sonar systems are predictable, such that automated tools like mbclean can be used to flag them as incorrect (Caress et al. 2010). Mbclean provides many options for flagging data depending on your survey area. The most common option is to flag a number of specified outer beams from both sides of the sonar array. Sound speed profile errors are usually larger in the outer beams along with a low signal-to-noise ratio (SNR). Of the four hundred beams found on the EM710 multibeam sonar only ten were flagged on both sides.

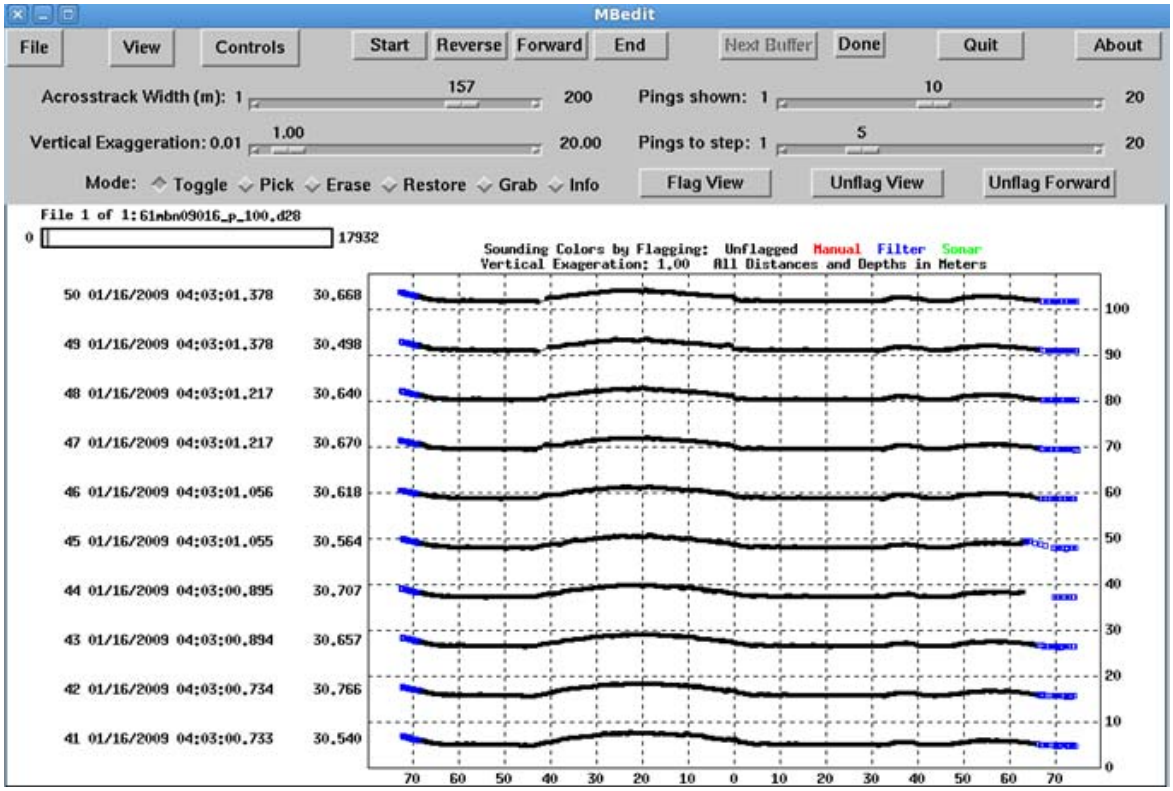

Figure 14. MB-systems mbedit tool

e. Applying to the Entire Data Set

At this point, only a small section (two line segments) of the data has been processed. This includes corrections for pitch and roll bias, a new sound speed profile, corrections to the navigation data, and the bathymetry data has been flagged. Then the MB-systems are used for the entire data set through the program mbset and mbprocess. Each data segment has a parameter file with default navigation, roll bias, and navigation settings. The mbset tool can quickly modify all the parameter files with the updated changes that have been made to the data. Mbprocess will then apply the modifications in each parameter file. The result is a new set of processed data files that can now be exported to Matlab for analysis. In order to analyze the data in Matlab, the processed data has to be in the correct format. The default mb-systems format for this data was ASCII. ASCII is limited format and only gives you a few points. Converting the data to binary provides a wider range over single precision floating point (FLT). The data is now in a double-precision binary FLT. Figure 14 shows the entire mb-systems data workflow.

B. ANALYSIS OF PROCESSED MULTIBEAM SONAR DATA

1. Bathymetry Data

a. Indexing Raw Multibeam Data

The main difficulty of bathymetry calculation using multibeam data is the spatial complexity itself. Sorting multibeam data requires significant computational capacity due to the large volumes of data and irregular sampling patterns. Using the geographic coordinates of each multibeam point, formatted into ASCII-style rows, the data are organized into 500 × 500-m geo-tiles, which are stored as direct-access files. A geo-tile index is then generated according to the grid subdivision method (Huang et al. 2008). Each index file consists of three components: a spatial header, a statistical matrix, and an index matrix. The header includes the spatial domain of the geo-tile, the grid interval of the geo-tile (e.g., 1 m), the grid size (e.g., 500×500m), and the maximum point numbers for all the grid cells. The statistical matrix stores the number of points in each grid cell, and the index matrix stores the record of the numbers of all multibeam points within each unit (1 × 1-m) cell. Using geo-tile index files for the proposed algorithm has

several advantages. First, an in-memory index for an arbitrary patch size can be calculated to speed the data searching mechanism used by least-square prediction (LSP). Second, the digital elevation model (DEM) terrain interpolation algorithms can rapidly search the raw data and compute distances. The geo-tile index can also be used to speed up multibeam data clipping over many geo-tiles in a rectangular area. After specifying the domain of a study area, a new sub-dataset can be extracted from the geo-tiles within the domain, and a corresponding index file can be generated, based on the same grid subdivisions (Huang et al. 2008).

b. Terrain Calculations

For terrain calculations, a 3-meter search radius is used in selecting multibeam points to interpolate the DEM by using the linear LSP method. The bathymetry depth Z_p for DEM grid point P can be given as

$$Z_p = cC^{-1}Z \tag{6}$$

where Z is a vector representing the depth relative to the seafloor trend of all the multibeam points within 3 meters $\{P_i\}$; this is written as

$$Z = \{Z_i\} = [Z_1, Z_2, \ldots, Z_n],\ n \leq 8 \tag{7}$$

c is a vector representing the covariance matrix between any interpolated point P and $\{P_i\}$, i.e.,

$$C = [C(\overline{PP_1})\ C(\overline{PP_2})\ \ldots\ C(\overline{PP_n})]^T \tag{8}$$

where $\overline{PP_i}$ is the distance between P and $\{P_i\}$ and $\overline{PP_i} \leq 3$m. C is the covariance matrix that represents the covariance between any two points in $\{P_i\}$, $C_{ij} = C(\overline{PP_i})$, which can be derived from the Gaussian function and written as

$$C_{i,j} = \begin{cases} \sigma_i^2 + C_{0,} & i = j \\ C_0\, e^{-c_1 d_{ij}^2}, & i \neq j \end{cases} \quad i, j = 1,2, \ldots, n \tag{9}$$

where d_{ij} is the distance between the i_{th} and j_{th} multibeam points P_i and P_j in $\{P_i\}$. σ^2_i is the accuracy measure associated with $\{P_i\}$. C_0 is the covariance for a distance of zero. C_1 is a parameter that controls the steepness of the covariance function, which can be determined from experience (e.g., 0.25) or estimated from the multibeam points $\{P_i\}$. If there is only one multibeam point within 3m for terrain interpolation, i.e., $N_{3m} <= 1$, the

depth of that DEM grid point is assigned as the depth of that multibeam point. On the other hand, if there are nine or more multibeam points within 3m (N_{3m} >= 8), only the nearest eight points will be included in the LSP terrain interpolation method (Huang et al. 2008).

2. Backscattering Data

a. Backscattering Strength

As mentioned in Chapter II, the EM710 provides two types of data. First data type is bathymetry; which we have already processed. The second type is backscattering strength. Processing the backscattering data is not as straightforward as the bathymetry data. The EM710 provides a great deal of seafloor backscattering information, which includes: angular variation and the absolute level of the power of the transmitted acoustic energy, absorption attenuation, angular response, beam pattern which is gathered through the receiver sensitivity (Teng 2011). Separating all this information is very difficult and provides an issue. Another issue lies with uncompensated sonar beam pattern residuals apparent in the backscatter angular response curve. Angular response will also affect the backscatter strength when you include seafloor geometry changes (Teng 2011). In addition, there are too many fluctuations in backscatter strength response signals when displayed in imagery. These fluctuations are not all due to the seabed response. Looking at the original image in Figure 15, it shows the transmitter source level generates a dark strip over the ships track. Some of these issues can be corrected using image processing software tools.

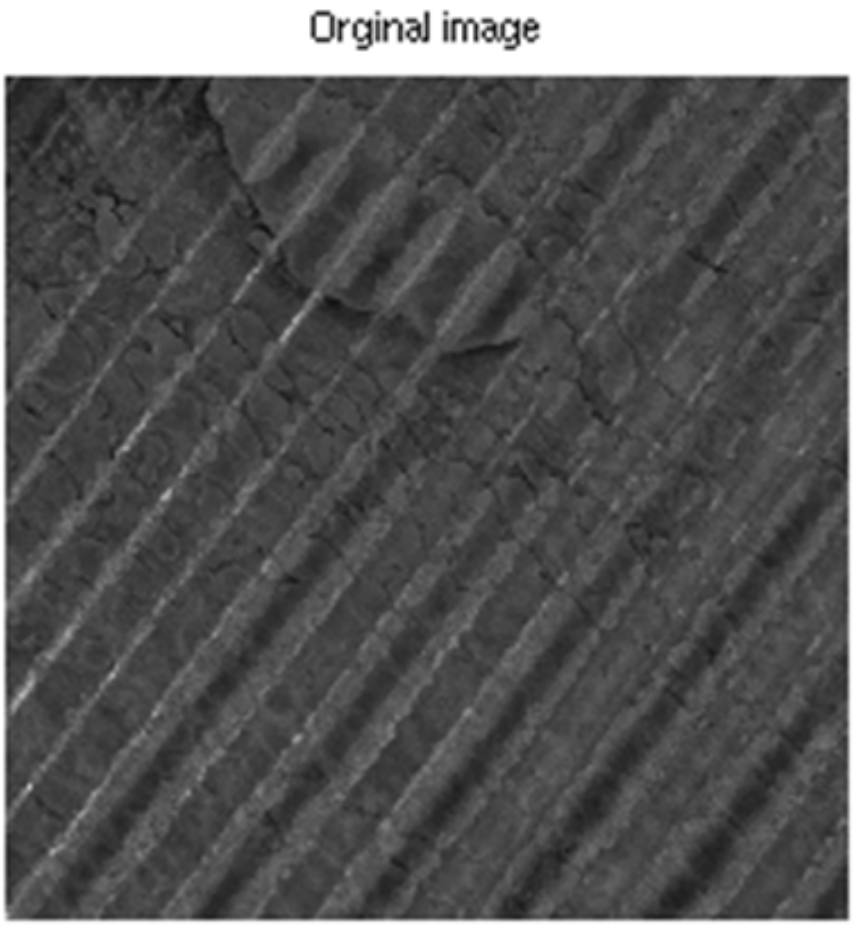

Figure 15. Original backscattering image

b. Frequency Domain Processing

Filtering using Discrete Fourier Transforms (DFT) makes it quite easy to perform image processing. Images can be expressed as sum of series of sinusoids of a signal. The sinusoidal pattern is broken up into three parts that capture all the information of an image; the magnitude, phase, and the spatial frequency. The magnitude is the difference between the brightest and darkest points. How the sinusoid is shifted relative to the origin is the phase. Frequency in the x-axis of the image is the spatial frequency. The Spatial frequency represents a value for each pixel in an image, while the magnitude is the brightness of each pixel. Fourier transforms encode a series of sinusoids; ranging

from zero to the maximum spatial frequency (resolution) of a digital image. The DC-component of an image is the average brightness. For a two-dimensional image with the size N x N, the DFT is:

$$F(k,l) = \sum_{i=0}^{N-1}\sum_{j=0}^{N-1} f(i,j)e^{-i2\pi\left(\frac{ki}{N}+\frac{lj}{N}\right)} \tag{10}$$

F (k, l) corresponds to each point in the Fourier space in the exponential term. *f (a, b)* is the image in the spatial domain. By multiplying the spatial image with the base function *F (0, 0)*, (DC-component) and the highest frequency function *F (N-1, N-1)* you obtain a value for each point *F (k, l)* (Fisher et al. 2004).

The inverse Fourier transform is as follows,

$$f(a,b) = \frac{1}{N^2}\sum_{k=0}^{N-1}\sum_{i=0}^{N-1} F(k,l)e^{i2\pi(\frac{ka}{N}+\frac{lb}{N})} . \tag{11}$$

Because the Fourier transform is separable, the result is

$$F(k,l) = \frac{1}{N}\sum_{b=0}^{N-1} P(k,b)e^{-i2\pi(\frac{ib}{N})}; \tag{12}$$

Using

$$P(k,b) = \frac{1}{N}\sum_{a=0}^{N-1} f(a,b)e^{-i2\pi(\frac{ka}{N})}. \tag{13}$$

The transform is used in Fourier filtering operations and can be done using several types of filters, i.e., low pass, high pass, and band pass filters. During the transformation the spatial domain represents the input and the output of the image is the frequency domain (Fourier). For this thesis, we focused on low pass filters. A low pass filter only allows low spatial frequency components to pass and removes all high spatial frequencies. This operation loses sharp crisp contours and only preserves broad smooth regions. In the Figure 16 you see four images; in the top left corner is the original plot. In this image, you can see the amplitude of the seafloor and the striping from the ships track. To the right and below the original image is the Fourier transform and the low pass filter

(mask). These are used to filter the striping from the original image. Finally, you have a filtered image, not as crisp as the original, but most of the striping has been removed.

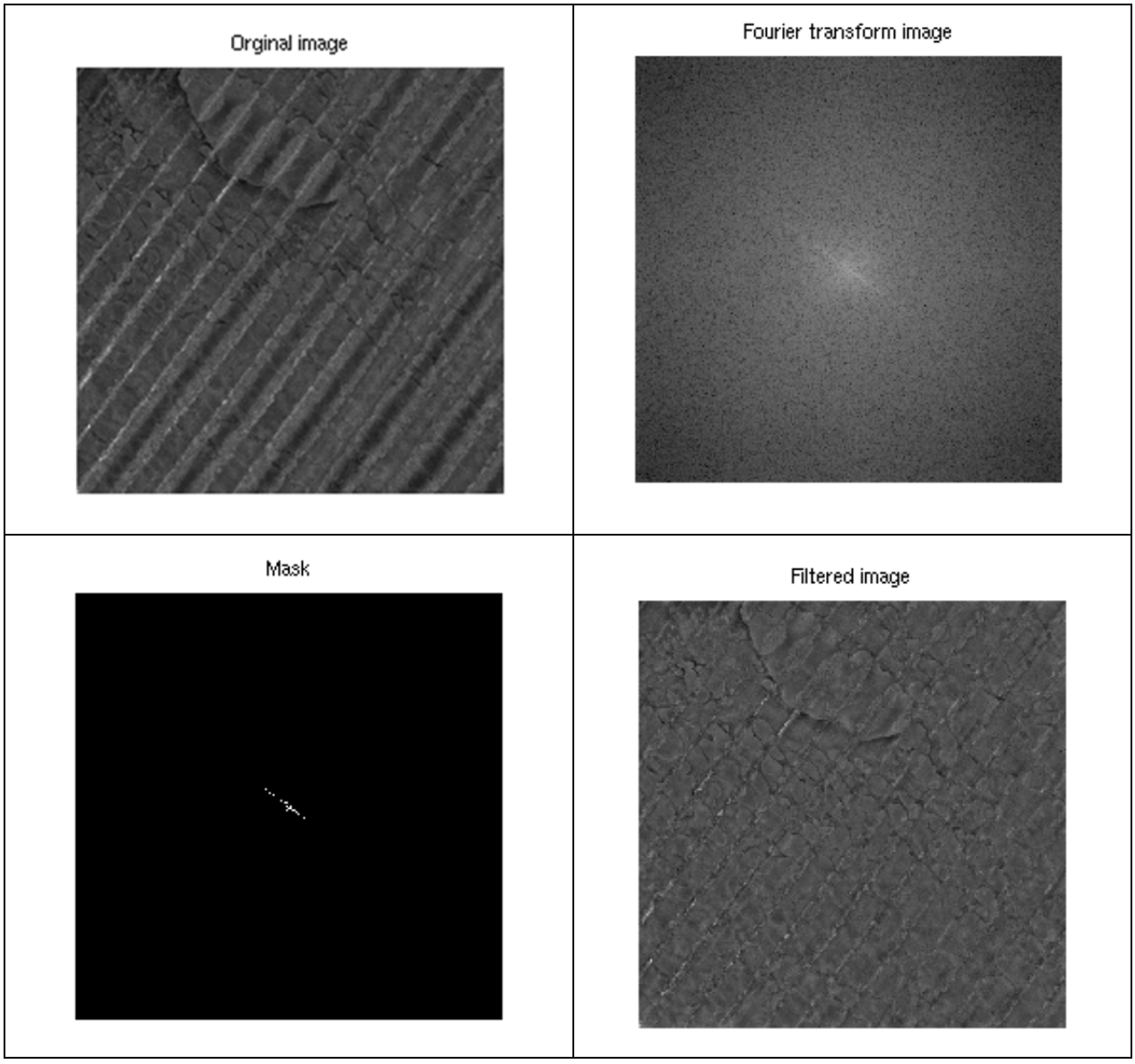

Figure 16. Fourier filtering process

THIS PAGE INTENTIONALLY LEFT BLANK

IV. MULTIBEAM ECHO SOUNDER DATA ANALYSIS

A. BATHYMETRY

Using the least square prediction program a grid can be generated and the binary float point values in ArcGIS native FLT files can be loaded into the new grid. Matlab can read the FLT data and convert it into a matrix. At this point, plots can be created using the data, along with 3D imagery. Figure 17 shows the bathymetry of the entire survey area at a 1-meter resolution. Depths range from 20 meters down to 60 meters. Average depth for this area is 42 meters. The western portion of the survey area has a dramatic change in depth due to the sloping downgrade. The island of Saipan is to the east of this plot. Figure 18 is a 3D bathymetry plot of the entire survey area. The northeast and southwest corners have the largest features that reflect the shallowest points. The western sloping downgrade is more easily seen here.

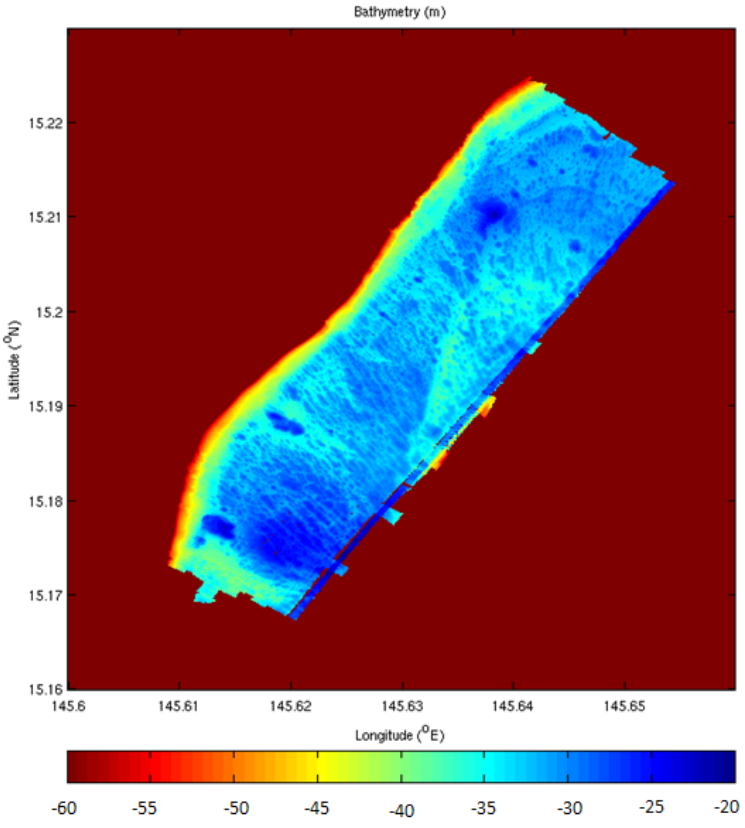

Figure 17. Bathymetry 1-meter resolution data

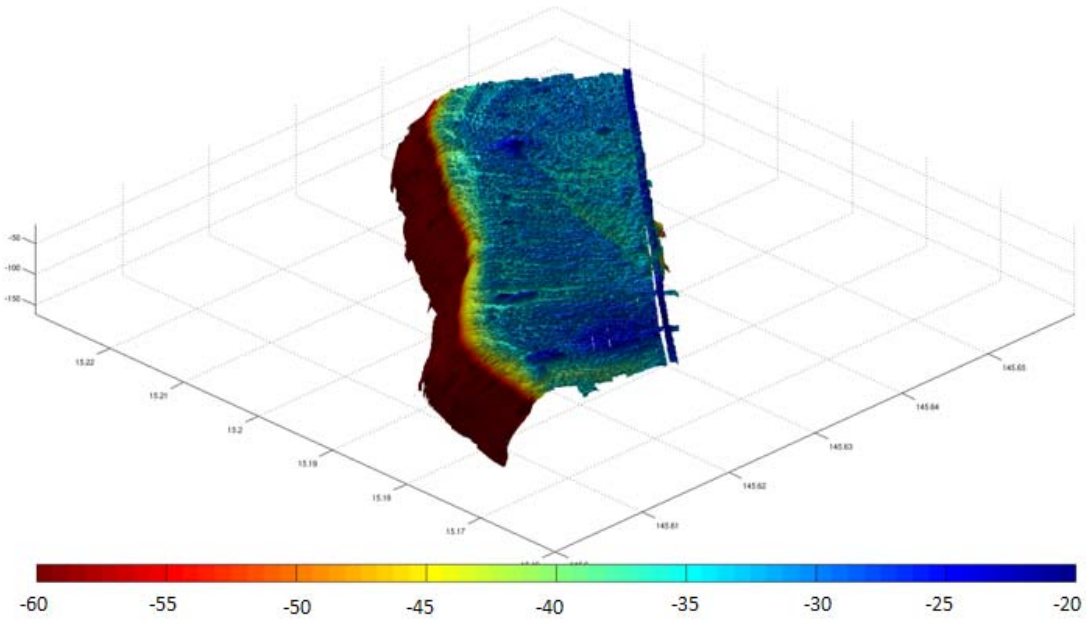

Figure 18. 3D bathymetry plot of the survey area

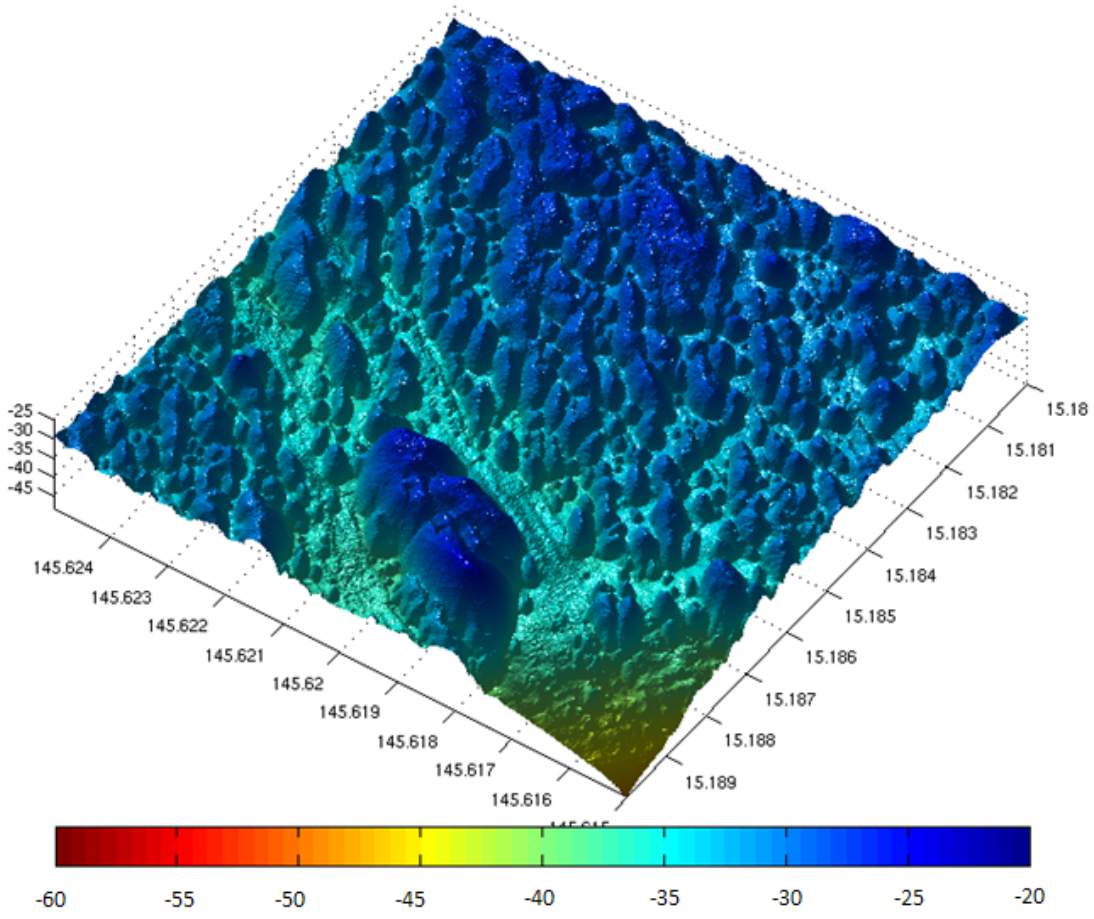

Figure 19. 3D bathymetry plot of an enlarged region

Figure 19 is 3D bathymetry plot of a single grid sector located in the southwest corner of the survey area. The terrain in this area is made up of mostly rocks with uneven surfaces. This terrain setup makes it an effective area to hide a mine. Here you can see a close up image of the terrain to compare to the roughness. Figure 20 is another 3D bathymetry plot of a single grid sector located in the southwest corner of the survey area, but with fictitious mines. The red dot represents a U.S. MK-75 bottom mine. The yellow dot represents a Chinese C-1 bottom mine. The dimensions of both mines are the actual size. This plot was designed to show the size of the mines compared to the landscape. The terrain with large concentrations of rocks makes it an effective area to hide a mine. While the open and smooth terrain where the MK-75 mine is located has a higher possibility of detection.

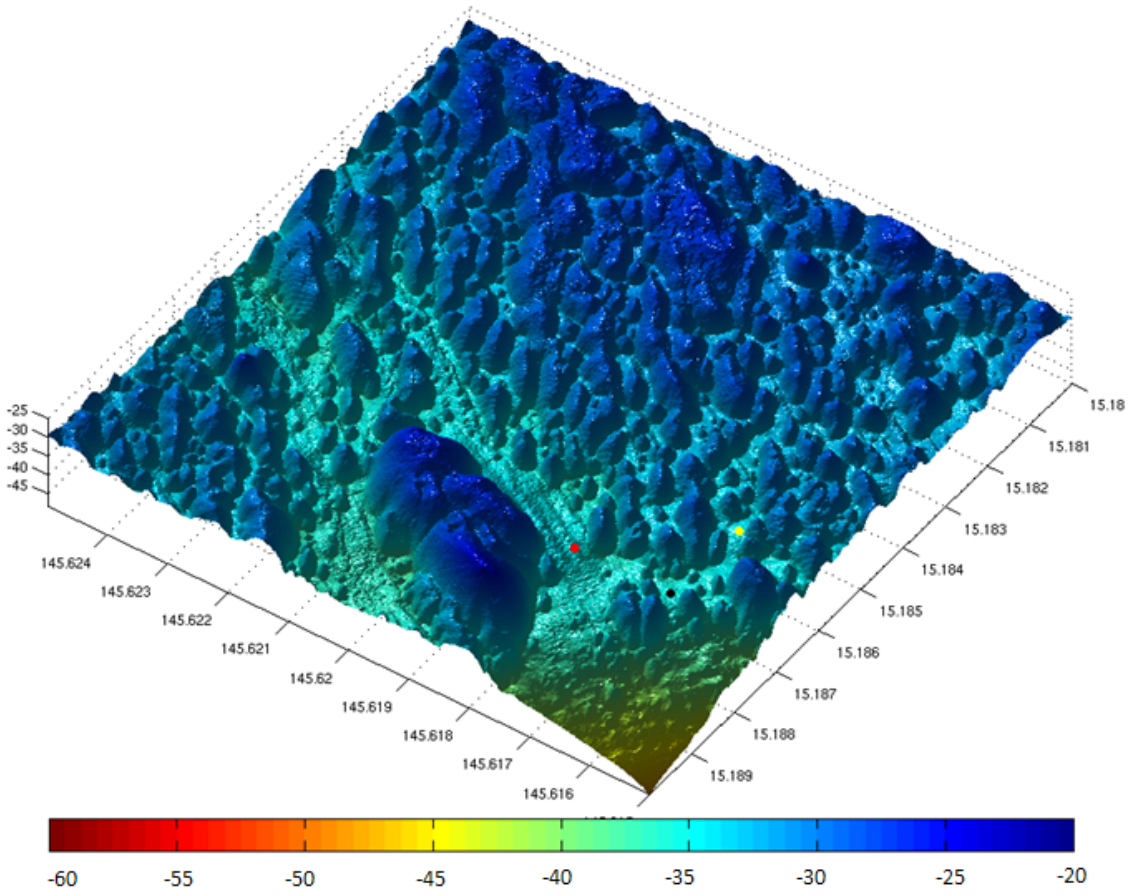

Figure 20. 3D bathymetry plot w/mines of an enlarged region

Figure 21 is a histogram of the raw bathymetry data before processing was completed. The x-axis represents all the possible depths and y-axis is the number grid points that have that depth. The depths range from 20 meters to areas with depths deeper than 200 meters. Figure 22 is a histogram of the 1-meter bathymetry data after processing was completed. The x-axis represents all the possible depths and y-axis is the number grid points that have that depth. The depths range from 20 meters to areas with depths deeper than 160 meters. During the processing, certain depths were removed in order to concentrate shallow area.

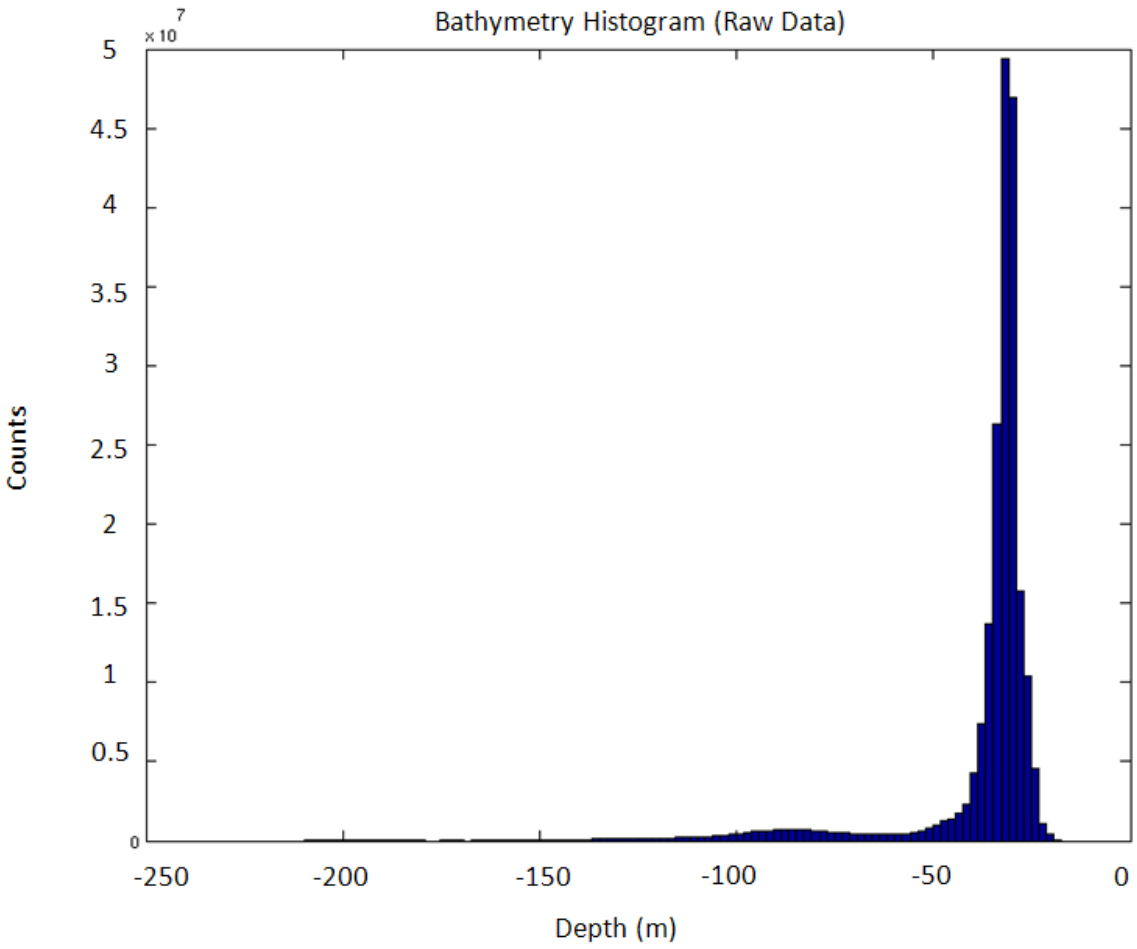

Figure 21. Histogram of Raw EM710 bathymetry data

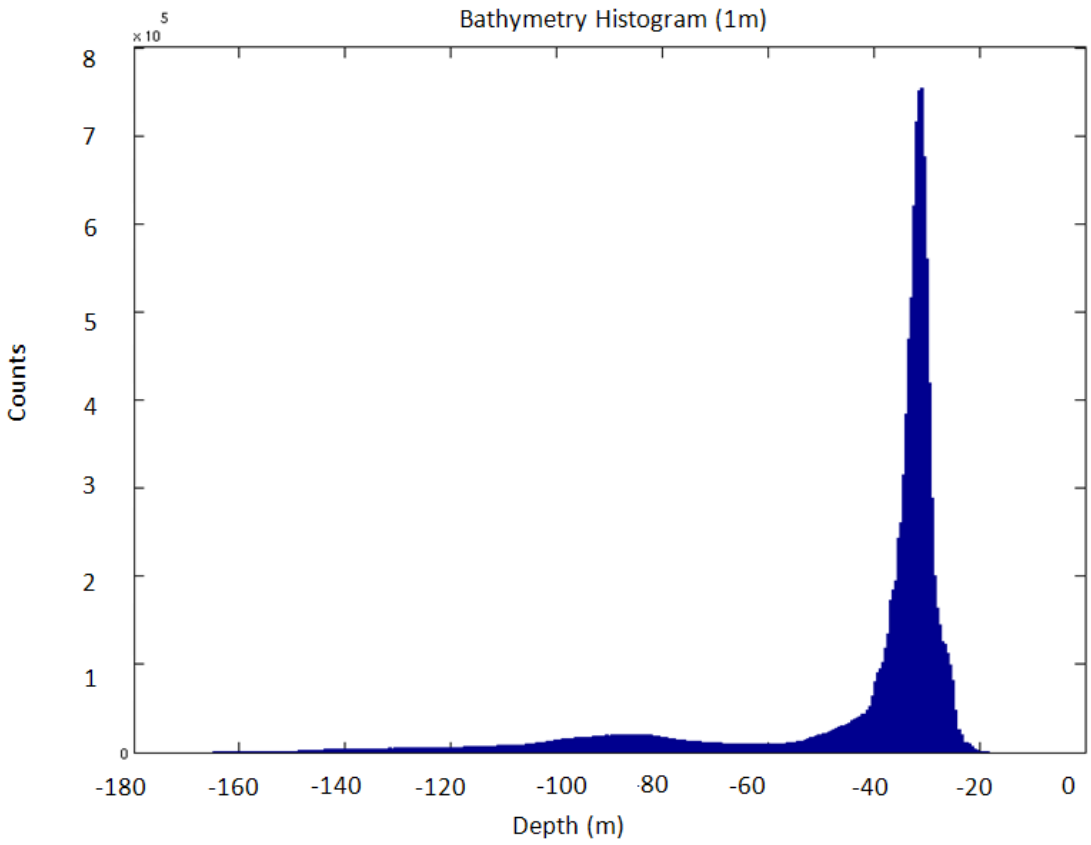

Figure 22. Histogram of 1-meter EM710 bathymetry data

B. BACKSCATTERING

The first step in building the backscattering plots is the same process as the bathymetry data plots. The second step entails using frequency domain processing to remove the striping from the plots. Utilizing the discrete Fourier transform and low-pass filter discussed in Chapter III, were able to remove most of the striping from the images. Figure 23, shows the difference between the original and filtered backscatter images. The two plots on top show the entire survey area. The blue rectangles designate the location of the two enlarged images on the bottom of Figure 23. The images show that with the removal of the striping the backscattering value is more accurate, but you sacrifice the crispness of the image.

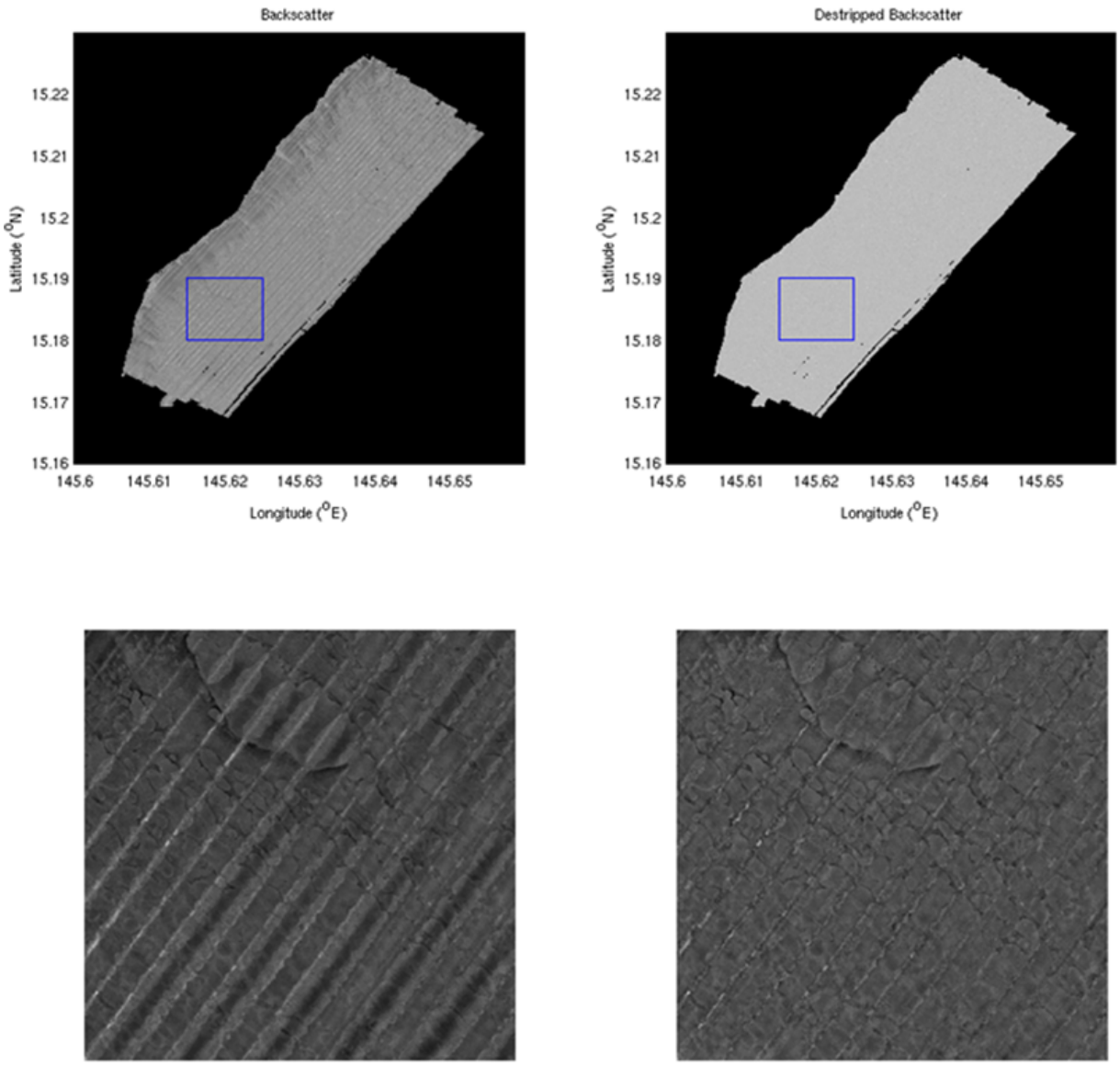

Figure 23. Backscattering data

Figure 24 is a histogram of the backscatter data. The x-axis represents all the backscatter raw values ranging from 0 to -70 (0 to -34 dB). The average raw value for backscattering is -20.9927 (-10.4964 dB).

$$Amplitude = Raw\ Value * 0.5\ (dB) \quad (14)$$

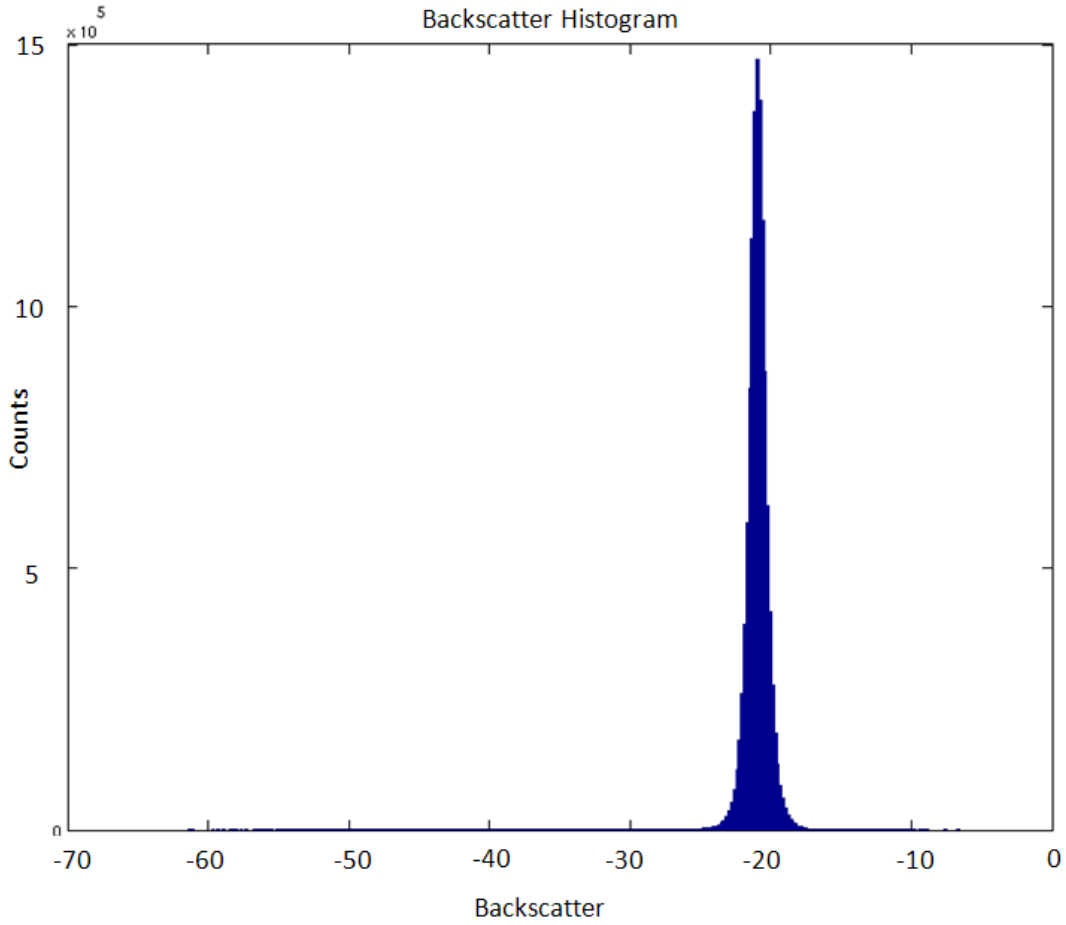

Figure 24. Histogram of backscattering data

V. NEW BOTTOM ROUGHNESS

A. REFERENCE LEVEL

Using 1-meter bathymetry data from EM710 and subtracting it from a 200-meter reference window, were able to determine a change in height between the seafloor (reference level) and the 1-meter terrain. The difficulty lies in trying to determine the true reference level of the seafloor to fit into the model. Large seamounts with flat surfaces provide an inaccurate trend of the actual seafloor. To correct for this, the reference level was calculated only using a portion of the survey area that did not contain any large seamounts. Figure 25 shows the 1-meter bathymetry data and the 200-meter reference bathymetry window used to calculate the new bathymetry grid. The blue rectangles designate the location of the two enlarged images on the bottom. This change in height provides us with a roughness value that can be applied to the current doctrine parameters mentioned in Chapter I.

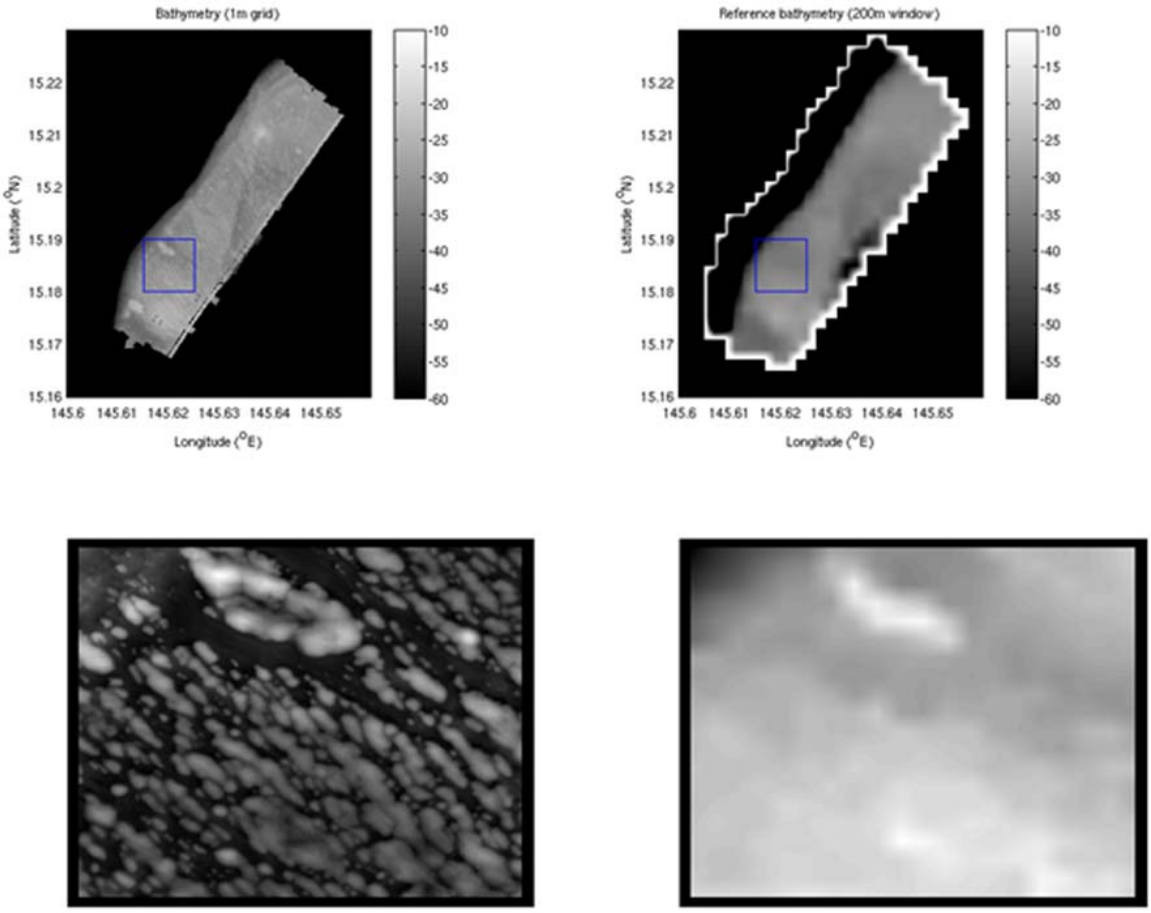

Figure 25. (a) Bathymetry from EM710, (b) calculated reference level from the data shown in panel (a) with a 200 m window, (c) EM710 bathymetry inside the box shown in (a), and (d) reference level inside the box shown in (b)

B. CONVERSION OF BATHYMETRY TO ROUGHNESS PERCENTAGE

The survey area is broken up into 25-meter grid boxes to look at the roughness each small grid in the test area. A threshold is required to calculate the objects i.e., rocks, gullies in the grid box. If the threshold is to low the objects can blend in with each other, making it look like one large object vice multiple objects. To determine the threshold required to accurately calculating the roughness, different thresholds were tested, this is illustrated in Figure 26.

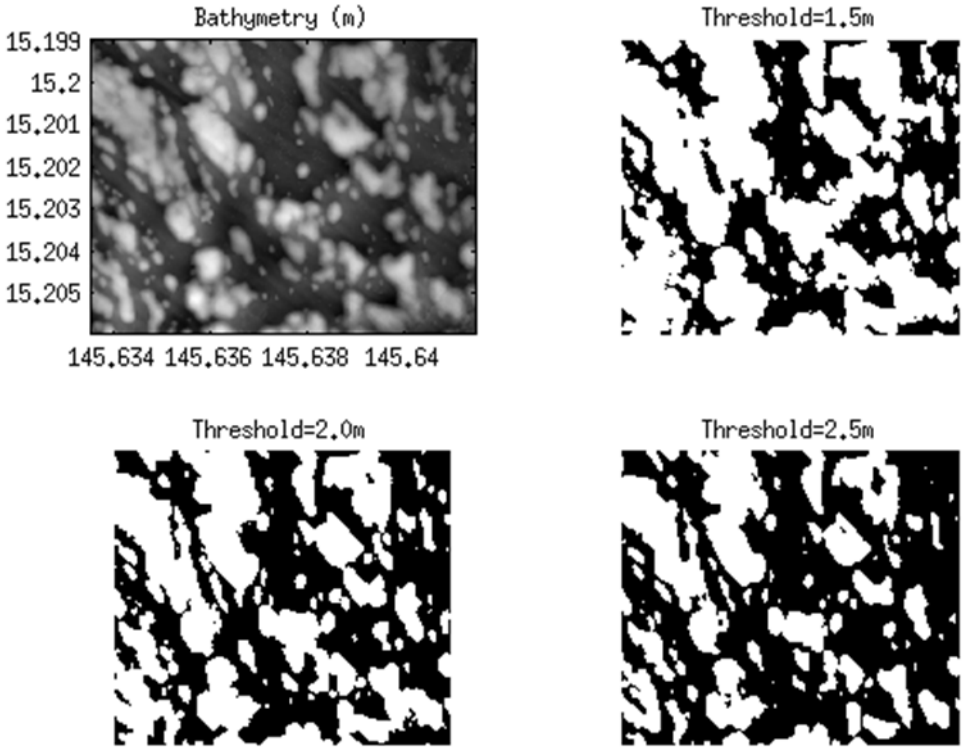

Figure 26. Threshold calculation

C. ROUGHNESS BY GRADIENT

The first partial derivative of a surface or the gradient can be used as a method of representing the bottom roughness of a terrain. The gradient provides two parameters: length and the direction. The elevations contained in a DEM can be described as a scalar field, in which the gradient is the vector field points in the direction of maximum variation. The Gradient vector length corresponds to the rate of change in that direction. Both parameters can be related to the slope and aspect of a surface of the seafloor. Usually the process is to compute the image derivative in the x-axis direction and in the y-axis direction. The combination of both directions will provide a vector. The depth gradient

$$|\nabla \bar{Z}| = \sqrt{\left(\frac{\delta z}{\delta x}\right)^2 + \left(\frac{\delta z}{\delta y}\right)^2} \tag{15}$$

is calculated from the EM710 bathymetry data using 8-connected neighborhood. To accomplish this calculation, we setup a matrix containing integers from 1 to 8, with m x n

elevation values (Figure 17). The *C* is the center of the 3 x 3 window shown in Figure 17. The direction is dependent on the slope counting clockwise from the top of the window. Figure 18 illustrates the process of determining the bottom depth gradient thresholds, based off bottom depth characteristics from EM710 bathymetry data.

8	1	2
7	C	3
6	5	4

Figure 27. Gradient matrix

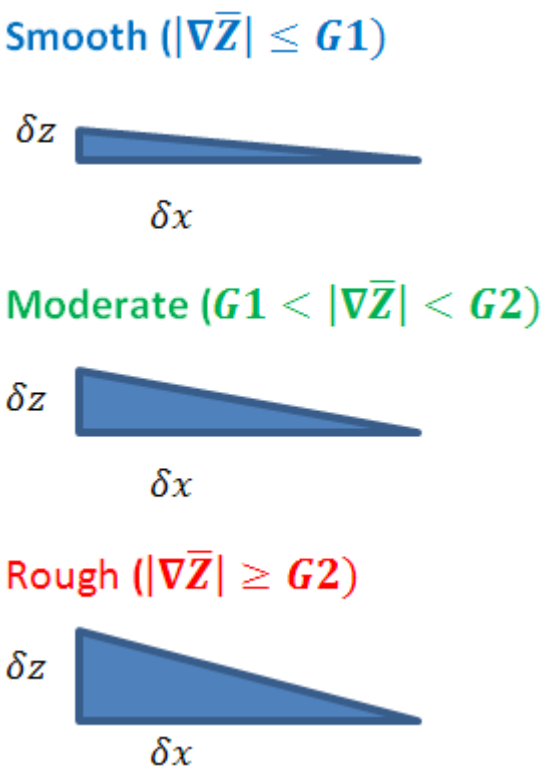

Figure 28. Bottom depth gradient thresholds for categories

D. ROUGHNESS BY MATHEMATICAL MORPHOLOGY

Another useful image processing tool for the analysis of binary images is mathematical morphology. The two fundamental operations of morphology are erosion and dilation. Erosion is the operation of removing boundaries of foreground pixels from a binary image. Dilation is the addition of foreground pixels to the boundaries of a binary image (Fisher et al. 2004).The structuring element also known as the *kernel* determines the number of pixels that are added or removed. The pattern of the kernel is specified as number of discrete points around an origin inside a two-dimensional grid. For this thesis, the structuring element was designed around a 3 x 3 window, as seen in Figure 29.

1	1	1
1	1	1
1	1	1

Figure 29. Structuring element window

Mathematical morphology can help enhance the roughness pattern of an image. The roughness of a binary image is the largest inter-cell difference of pixel in the center of the image and the surrounding boundary cells (Schwanghart and Kuhn 2010):

$$Roughness = Max[(ID(DEM, k) - DEM), (DEM - IE(DEM, k)] \quad (16)$$

where:

ID = Image Dilation

IE = Image Erosion

k = kernel

DEM = Digital Elevation Model

THIS PAGE INTENTIONALLY LEFT BLANK

VI. RESULTS

A. ROUGHNESS REQUIRING REFERENCE LEVEL

1. DBDB-V as the Reference Level

The first type roughness (R1) was planned to be calculated by subtraction of the Digital Bathymetric Data Base – Variable Resolution (DBDB-V) from the EM710 data with 1 m resolution. Here, the DBDB-V, used as reference level surface, is bathymetric database at different resolutions. For example 0.05 minute resolution requires level 3 classification. Data from Level 0 was used to keep this thesis unclassified and available for public release (NOAA 2011).

Level	*Classification*	*Release*
Level 0	Unclassified	Public Release
Level 1	Unclassified	No Public Release Data
Level 2	Classified	No Public Release Data
Level 3	Classified	No Public Release Data

Table 3. DBDB-V levels of classification and detail

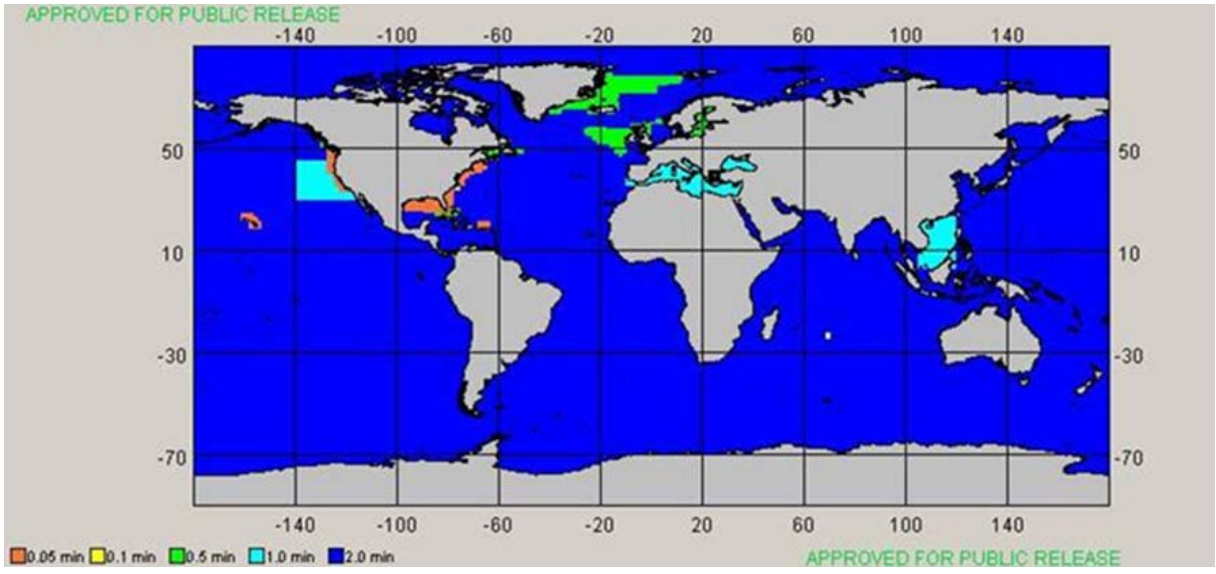

Figure 30. Level of resolution available for each area of the world (From NOAA 2011)

Unfortunately, the only data available in the pacific area off Saipan is 2.0 minute resolution. The higher resolution is only in select areas as seen Figure 28. 2.0 minute data does not use contour intervals less than 100 meters. Plotting the roughness using 100 m resolution data will not accurately show the true roughness.

2. Filtered Bathymetry as the Reference Level

The second roughness (R2) created incorporates the Navy Current Doctrine and uses the least square prediction program. Figure 30 is plot of the new bathymetry grid for R2 over the entire survey area. The blue grid box represents a smaller test area seen in Figure 31. To determine the roughness in the test area the trend was removed.

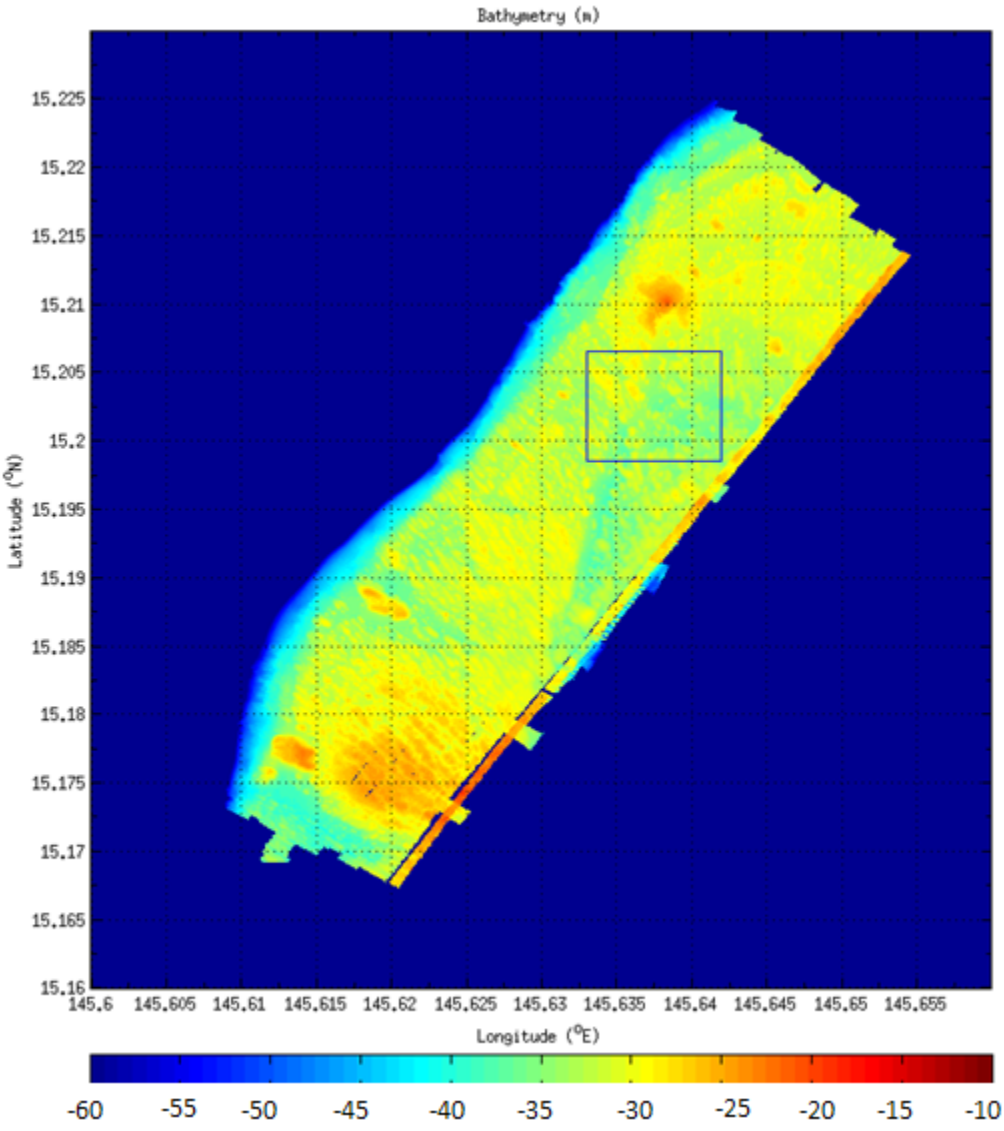

Figure 31. The bathymetry (m) for the whole area. The blue box is the enlarged area shown in Figure 31

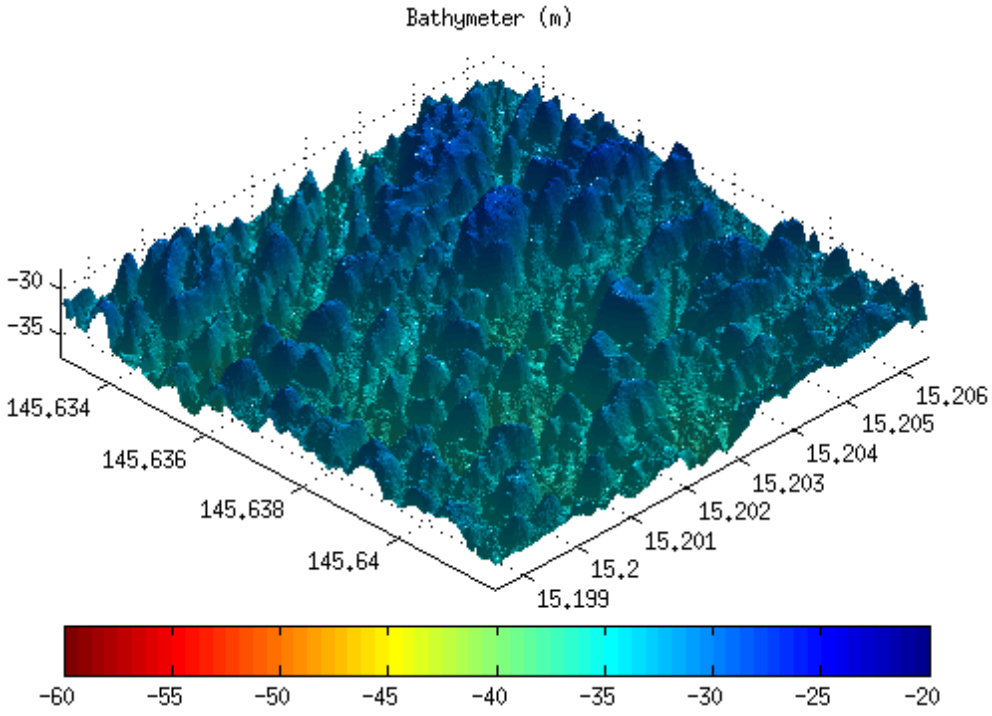

Figure 32. Enlarged 3D bathymetry plot of the R2 tested area

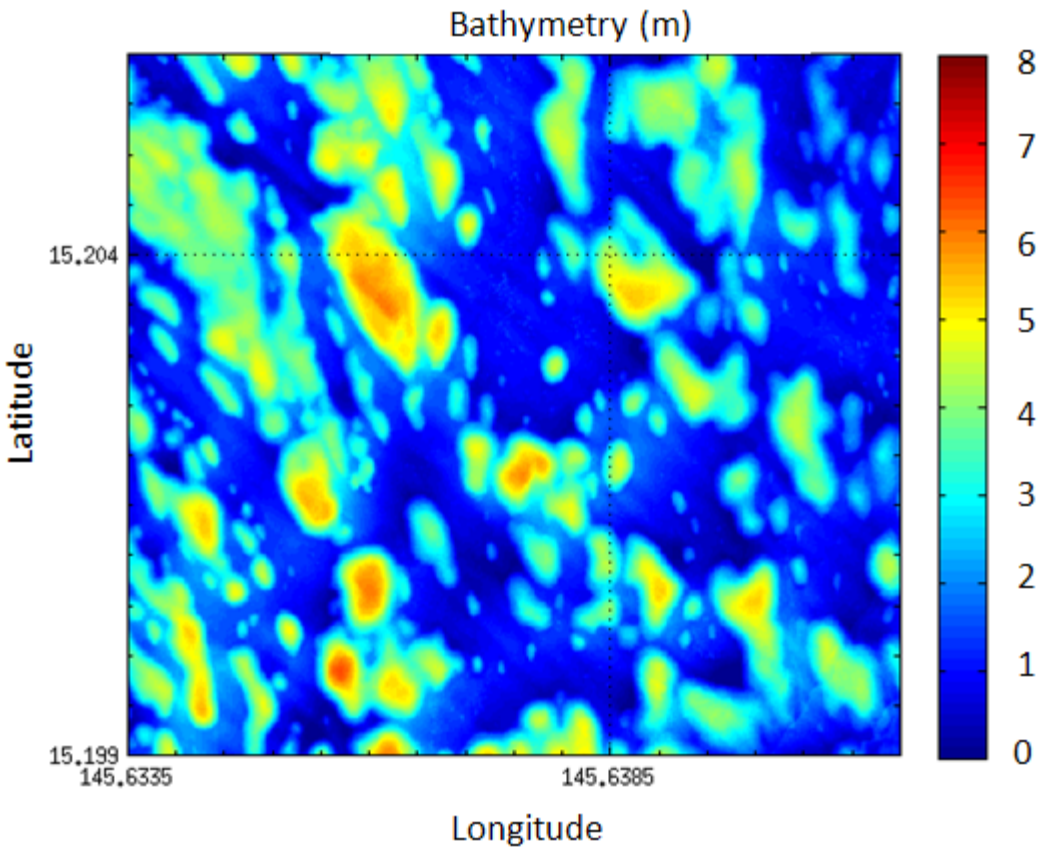

Figure 33. Test area with trend removal

Using a 2.5-meter threshold shown in chapter IV Figure 26, the roughness for the test area can be determined for the bottom roughness calculation. By the current Navy doctrine, this entire test area contains over 38% roughness objects, making it bottom profile group rough. This generalization is too broad and does not show any detail. To improve on the doctrine, we broke up the test area into 25-meter grid boxes and tested the rough percentage for each box. Figure 34 is the roughness percentage calculation for each grid box inside the test area for R2. The blue color grid boxes signify the smooth roughness category, green is the moderate category, and the red areas are the rough category. We know the area is mostly rough, but instead of just classifying the area rough we can show the areas that are smooth and moderate. Figure 35 is a bar chart of the three roughness categories for the R2 test area.

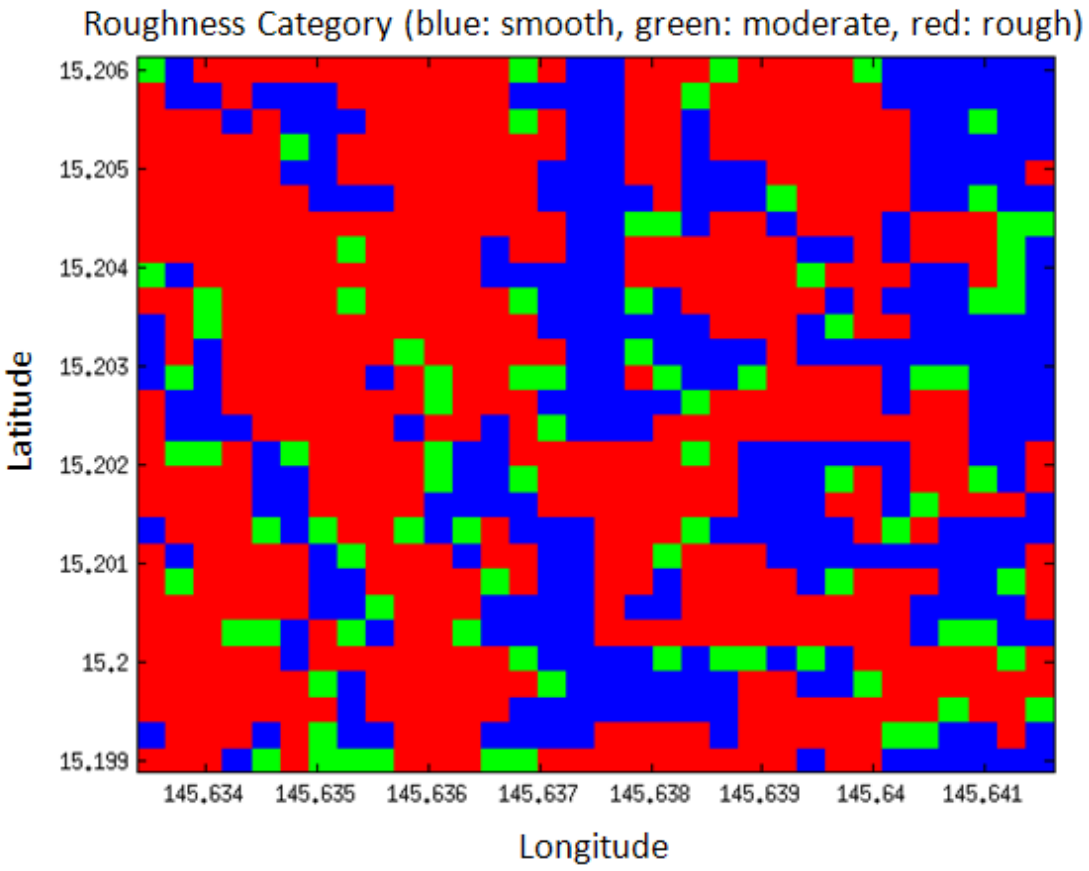

Figure 34. Roughness categories over the test area

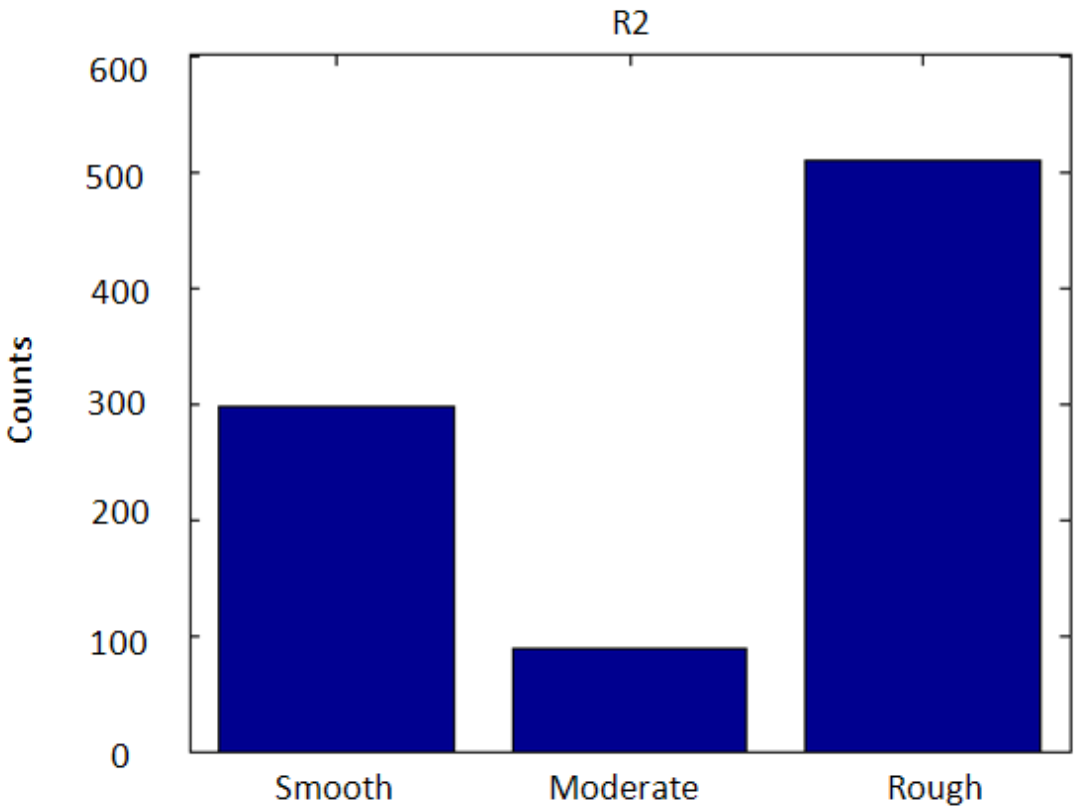

Figure 35. Histogram for the R2 Categories with the current Navy doctrine

B. ROUGHNESS NOT REQUIRING REFERENCE LEVEL

1. Roughness with Depth Gradient

The third type roughness (R3) is on the base of depth gradient from EM710 with1 m resolution. The benefit of this method is no reference level to be required. With the Topo Tool Box gradient8 Matlab functions, accurate depth gradient is calculated to represent the bottom roughness (Schwanghart and Kuhn 2010). Figure 36 shows the gradient of the EM710 survey area. Similar to the current Navy doctrine, the depth gradient (R3) can also be divided into the smooth/moderate/rough categories with thresholds. To accomplish this task, we used the bottom depth gradient threshold model shown in Figure 18 in Chapter IV. The results were the gradient threshold values found in Table 4.

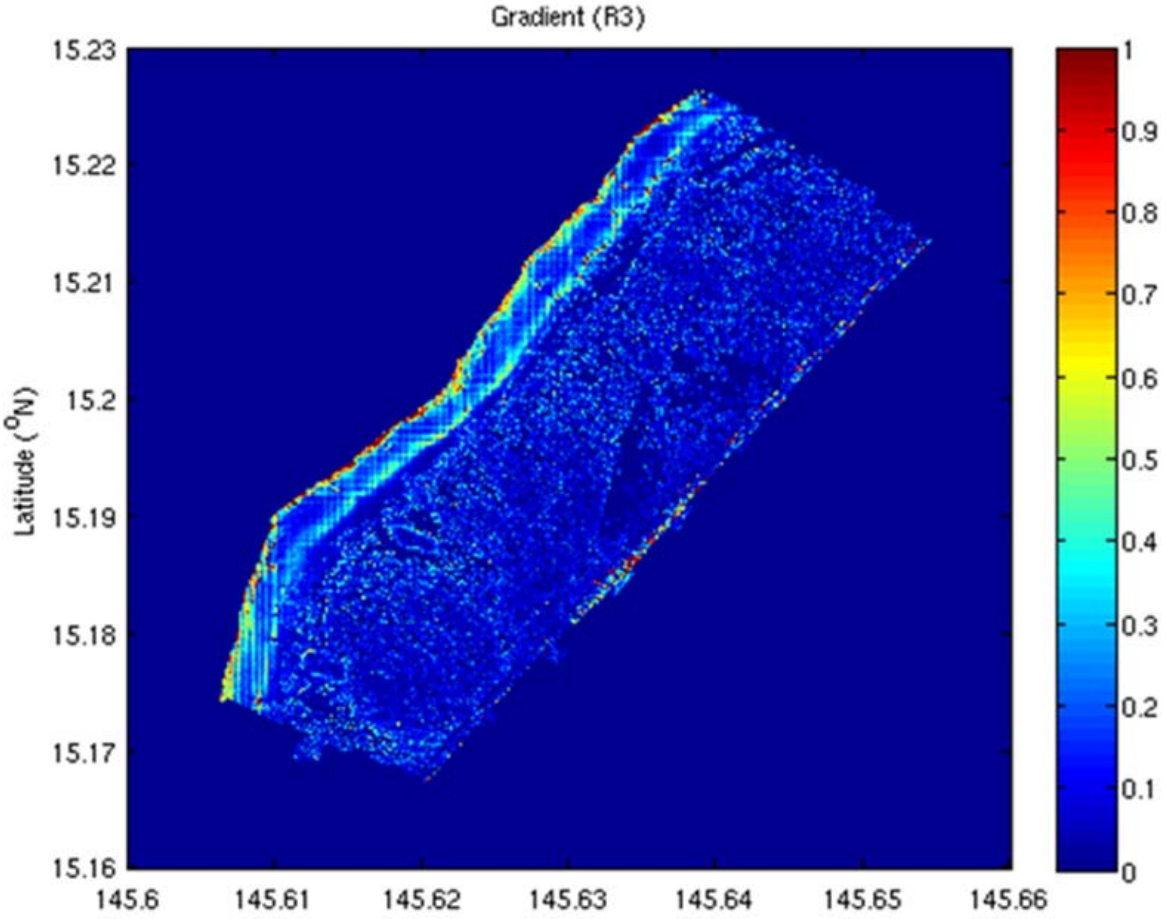

Figure 36. Depth gradient

Roughness Category	***Bottom Depth Gradient Thresholds***	
Smooth	$0 < \lvert\nabla\bar{Z}\rvert < G1$	G1 = 0.05 G2 =0.15
Moderate	$G1 < \lvert\nabla\bar{Z}\rvert < G2$	
Rough	$G2 < \lvert\nabla\bar{Z}\rvert$	

Table 4. New roughness category comparable to the current Navy doctrine

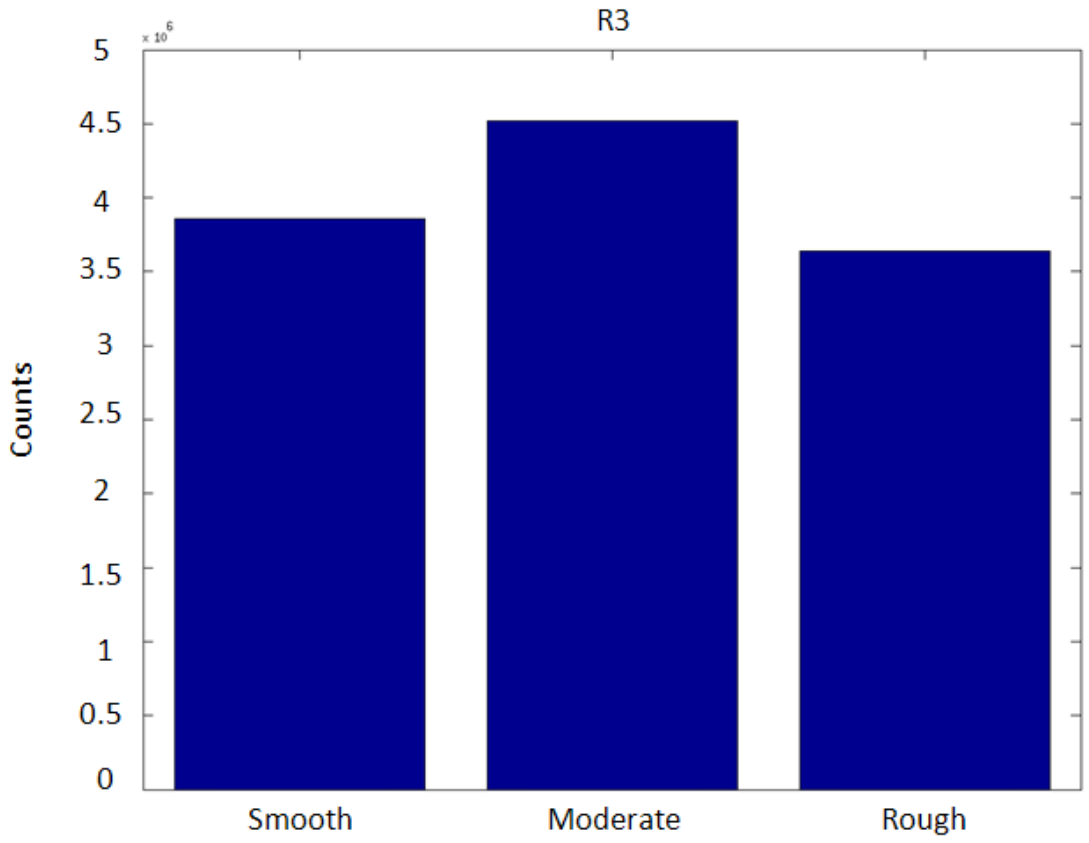

Figure 37. Histogram of bottom roughness categories of gradient (R3) for the whole area

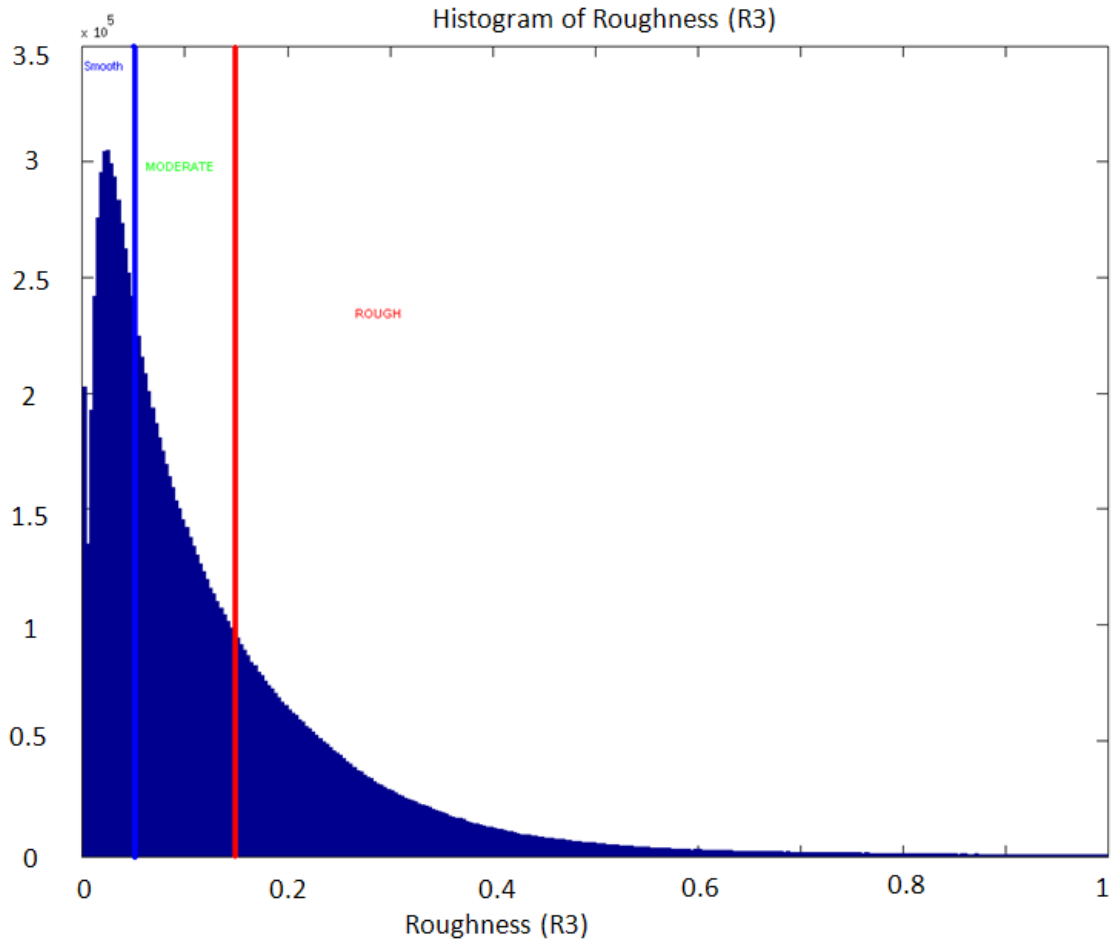

Figure 38. Histogram of the bottom depth gradient from EM710 bathymetry for the whole area

Figure 39 shows the three roughness categories from the gradient data plotted over the entire area. The blue color signifies the smooth terrain, green is the moderate terrain, and the red areas are the rough regions.

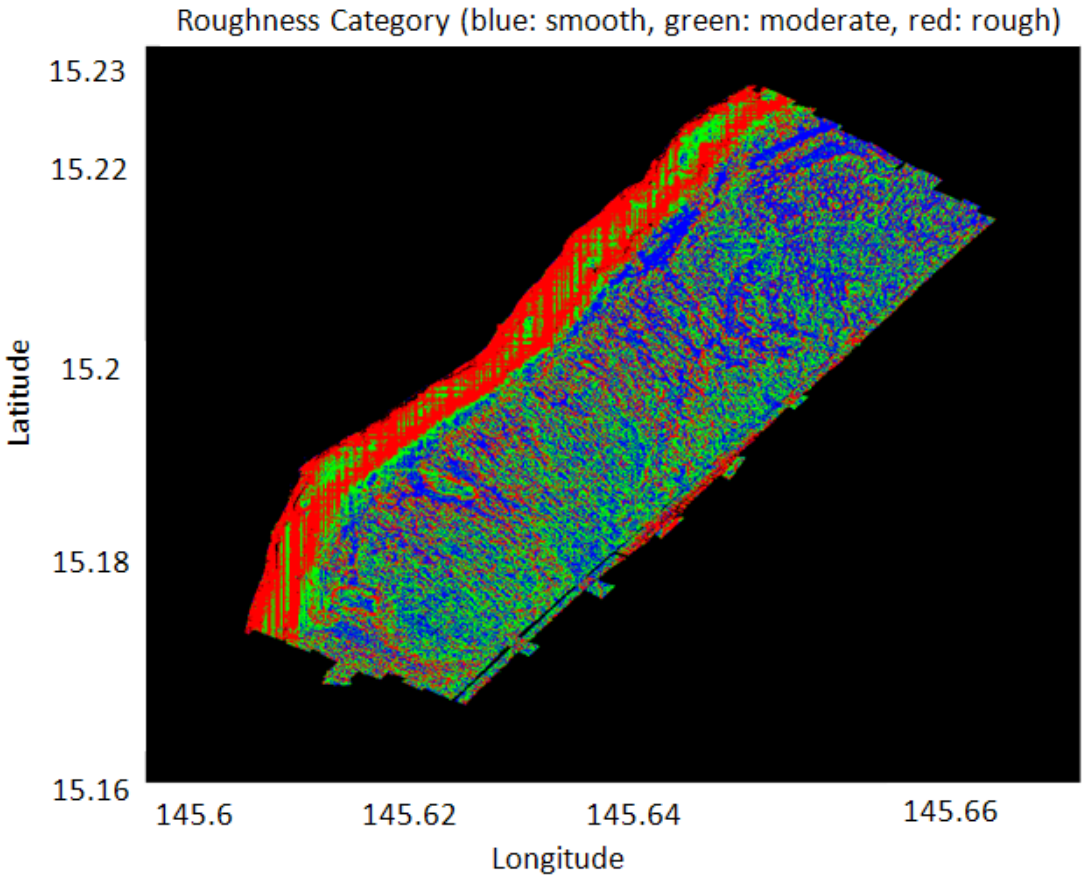

Figure 39. Roughness categories from gradient calculation of the whole area

To compare it to R2; we also created gradient plots of the R2 test area. Figure 40 is the gradient plot of the test area. Here you can see R3 provides a more detailed roughness reference than seen in Figure 34 for R2 in the shallow water. Figure 41 is the bar chart for the R3 Gradient test area. The bar chart illustrates the test area has more smooth areas than rough, but because of the current doctrine the entire area would categorized as rough.

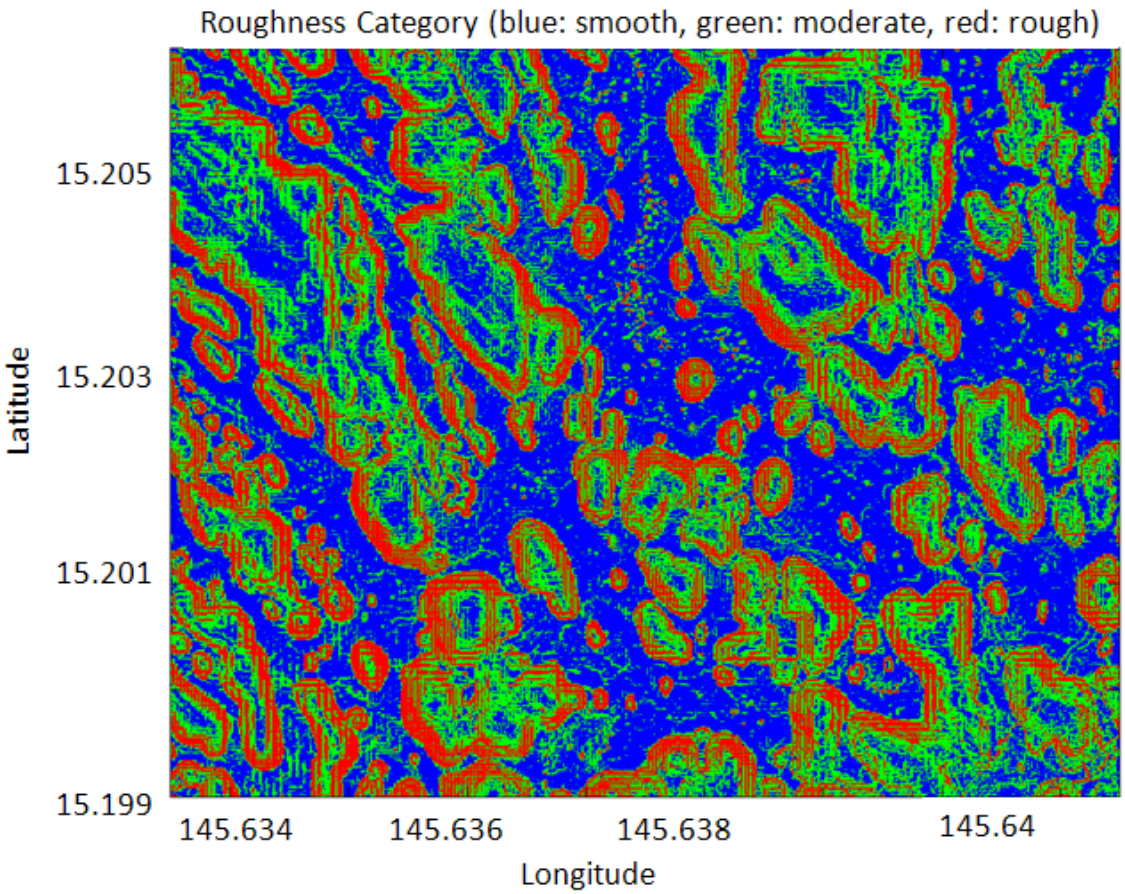

Figure 40. The Gradient of the R2 test area

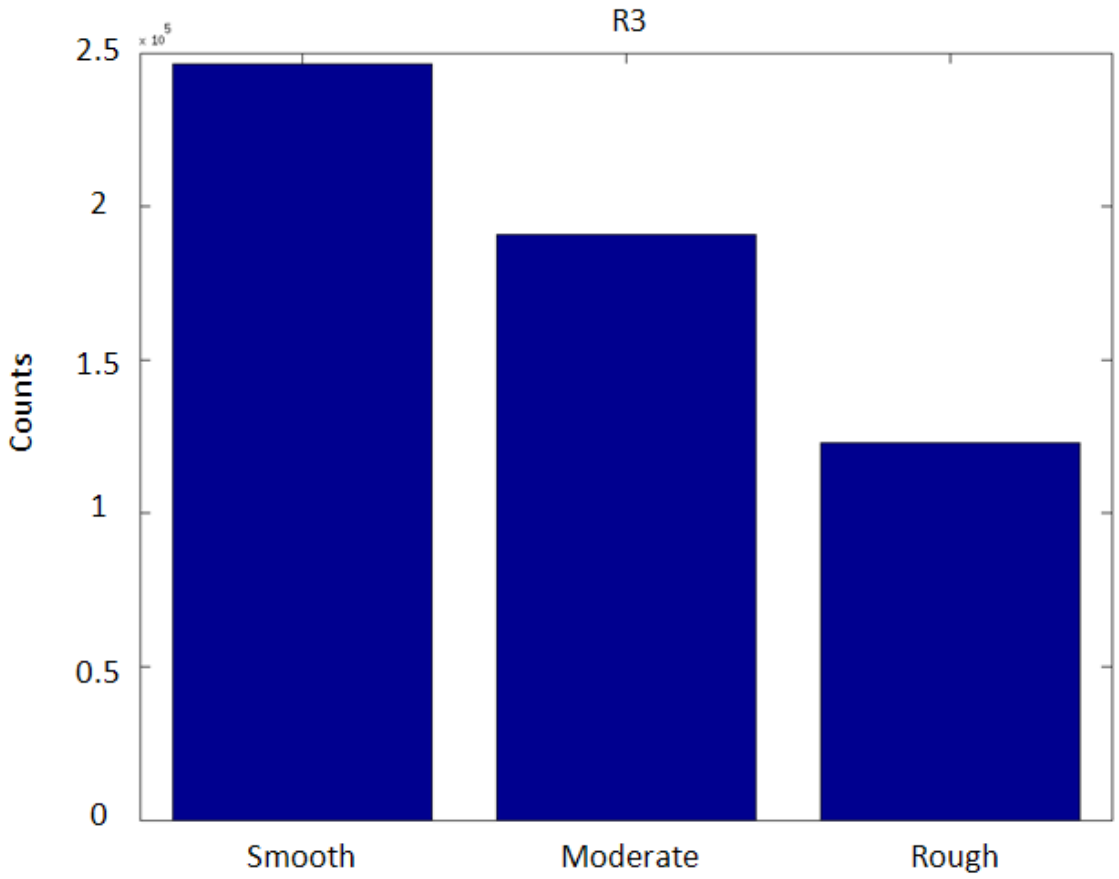

Figure 41. Bar chart of the Gradient in the R2 test area

2. Roughness with Mathematical Morphology

The fourth type bottom roughness (R4) is calculated from EM710 with the mathematical morphology. Topo tool box has Matlab functions for calculating the roughness of terrain using the EM710 1-meter bathymetry data and the morphology equation mentioned in Chapter IV (Schwanghart and Kuhn 2010). The output is a new roughness data that is plotted in Figure 42. Similar to the depth gradient (Figure 36), morphology (R4) can also be divided into the smooth/moderate/rough categories with thresholds. To accomplish this task, we used R4's bar chart seen in Figure 43 and modeled the category thresholds off R3's bar chart to match similarly. The results were the morphology roughness threshold values found in Table 5.

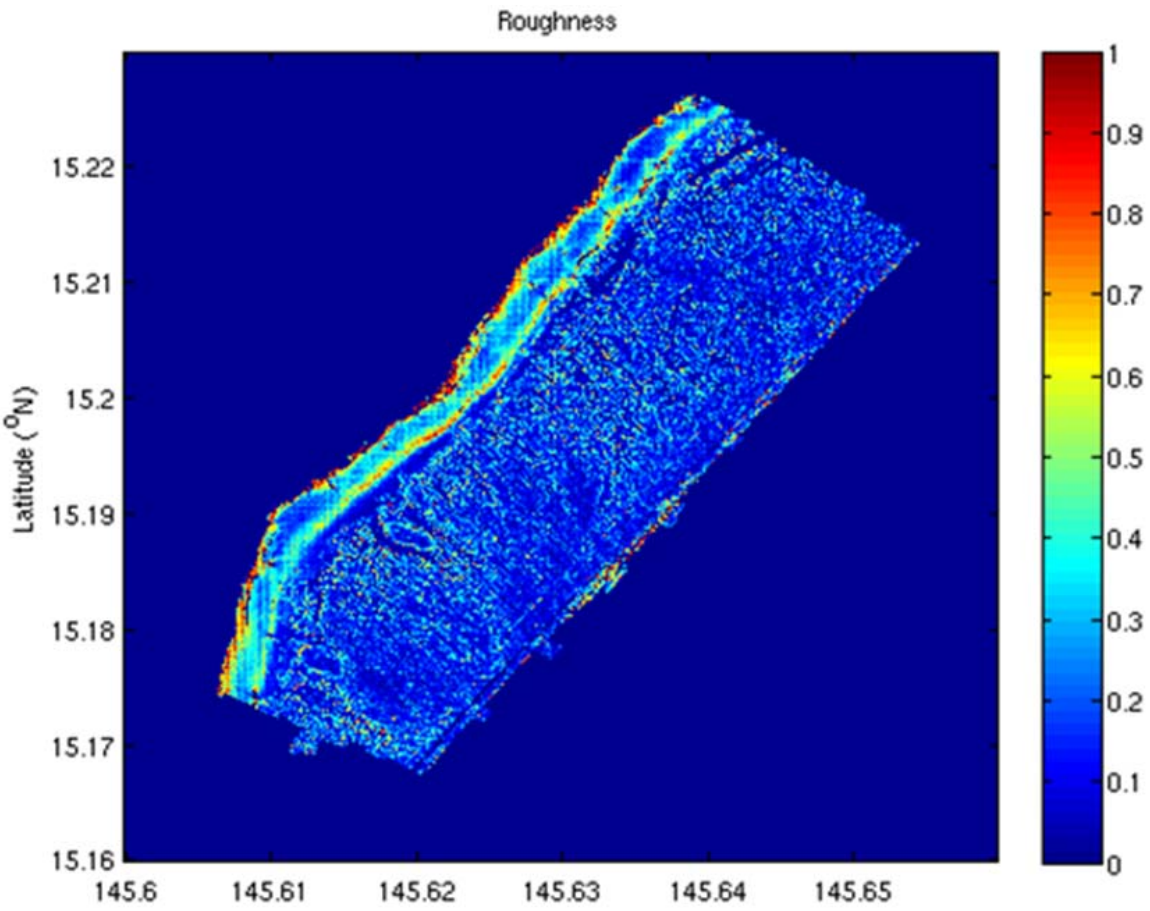

Figure 42. Fourth type bottom roughness (R4)

Roughness Category	***Bottom Roughness Morphology***
Smooth	Less than .09
Moderate	Between .09 and .24
Rough	Over .24

Table 5. Roughness threshold parameters (R4)

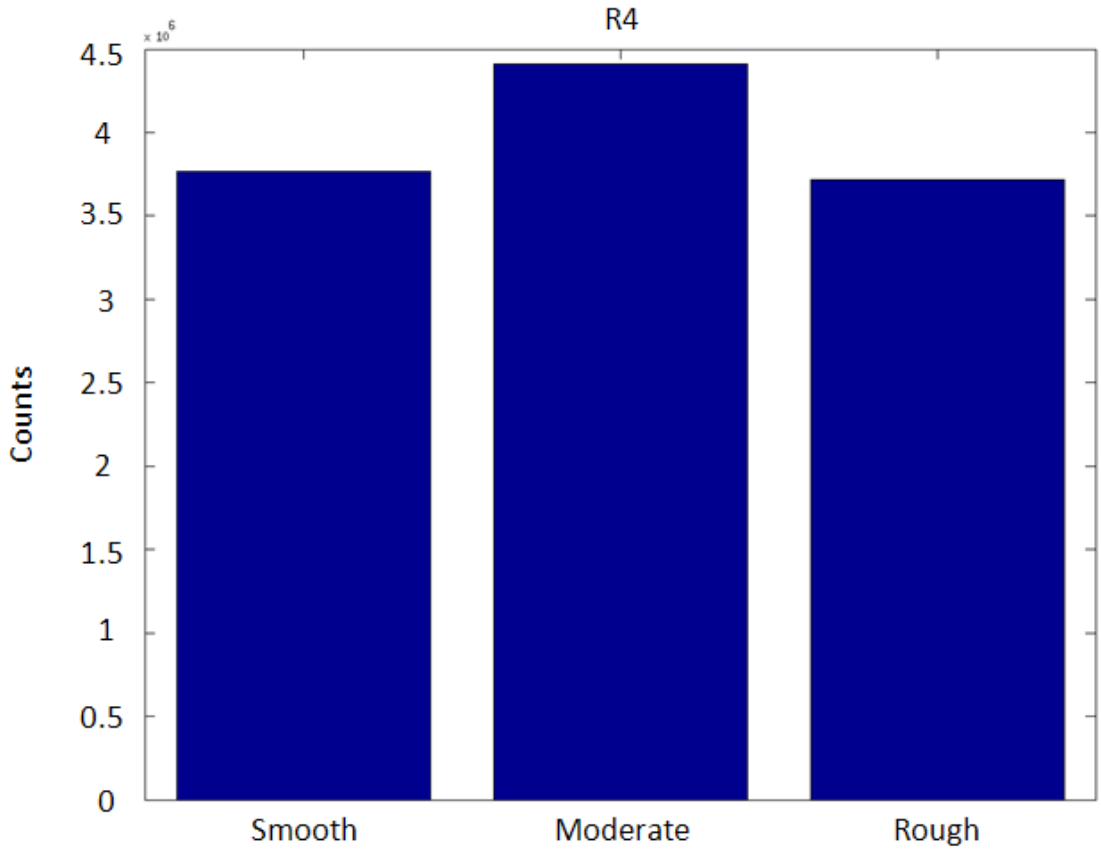

Figure 43. Bar chart of roughness (R4) over the whole area

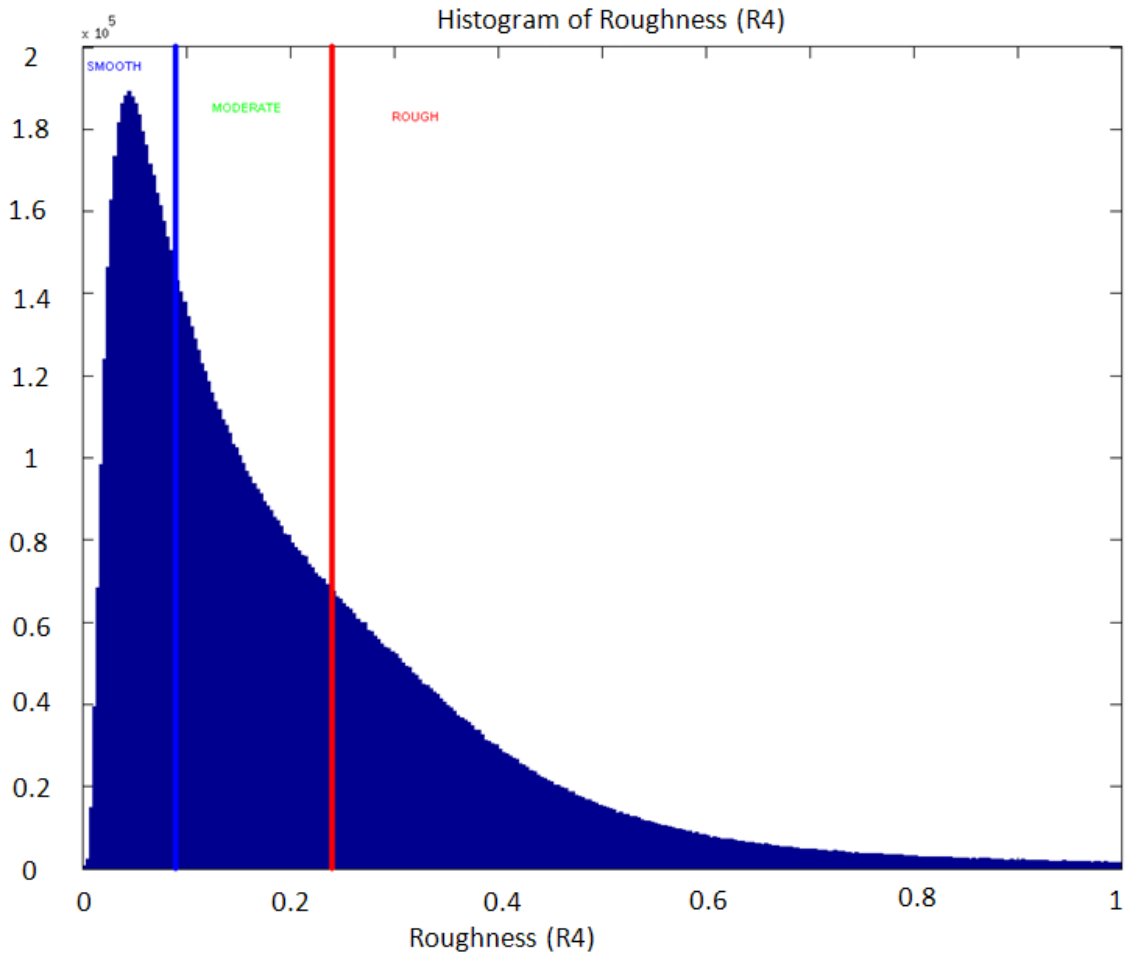

Figure 44. Histogram of roughness (R4) over the whole area

Figure 45 shows the three roughness categories from the gradient data plotted over the entire area. The blue color signifies the smooth terrain, green is the moderate terrain, and the red areas are the rough regions. The R4 plots are quite comparable to Figure 37, 38, and 39 for R3.

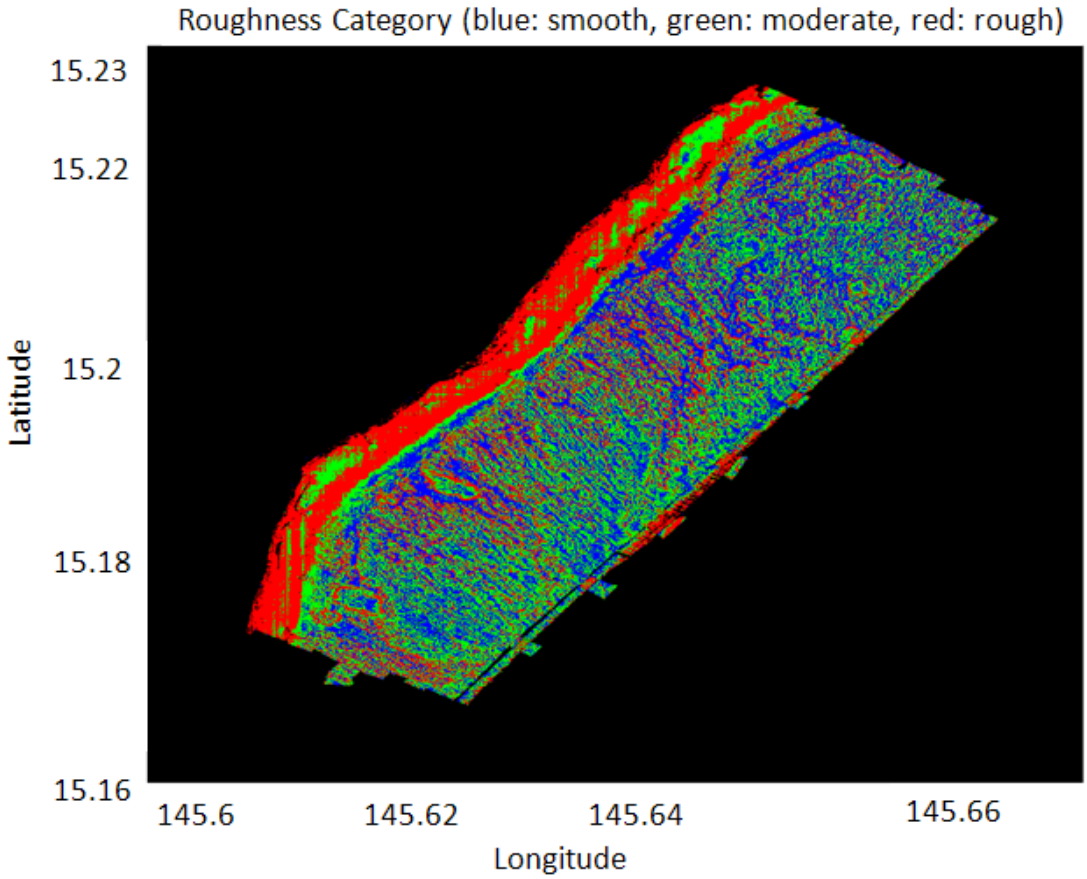

Figure 45. Roughness categories from the mathematical morphology calculation (R4)

A comparison of the R2 test area was also done utilizing mathematical morphology (R4). Figure 46 is a plot of the roughness in the R2 test area using the mathematical morphology method of calculating roughness. Figure 47 is a bar chart of the roughness.

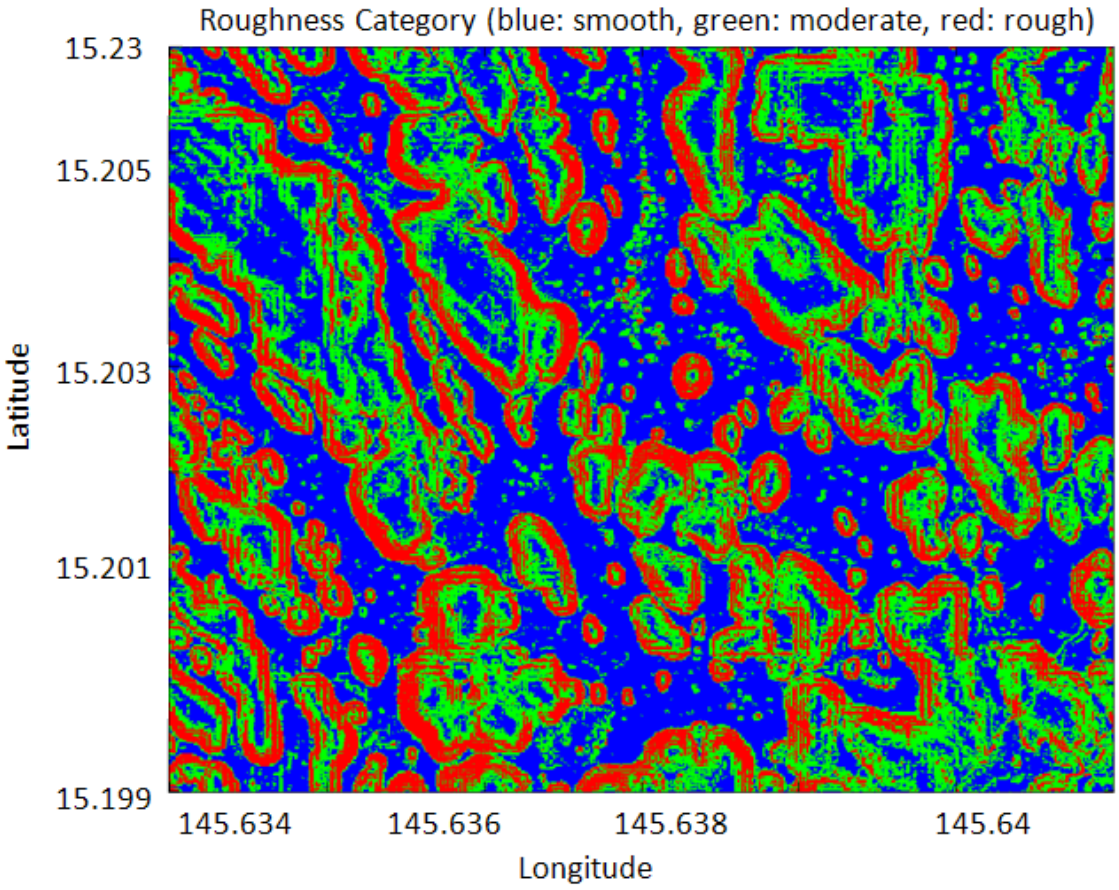

Figure 46. Mathematical Morphology of the R2 test area

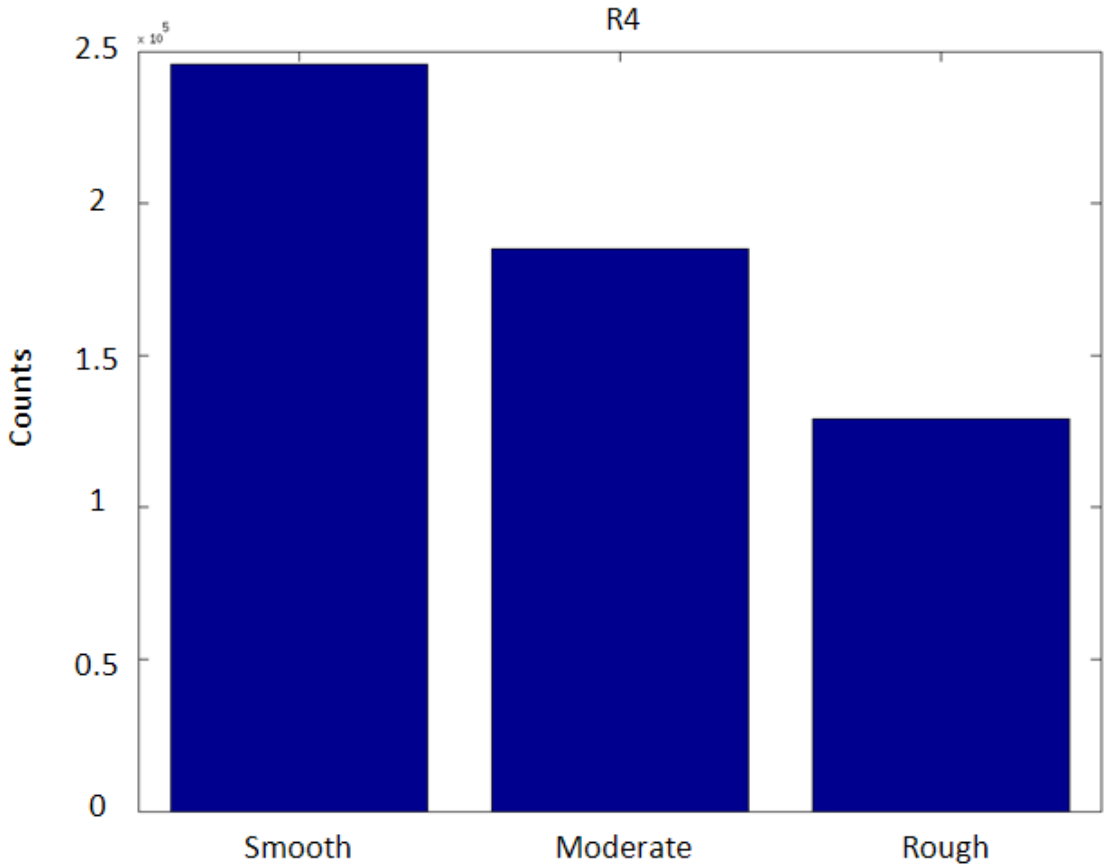

Figure 47. Bar chart of the roughness categories in the R2 test area using the R4 method

C. DATA STATISTICS

EM710 Bathymetry/Roughness Data Statistics

Raw Data	
mean	-36.7294
min depth	-17.5
max depth	-209.8
STD	16.9983

1 - Meter Data	
mean	-42.1689
min depth	-18.31
max depth	-165.05
STD	23.6607

R2 (Change in Depth)	
mean	10.0262
min	-10
max	64.0503
STD	12.1753

R3 (Gradient)	
mean	0.1397
min	0
max	1
STD	0.2219

R4 (Roughness)	
mean	0.2293
min	0
max	1
STD	0.3437

Figure 48. EM710 Bathymetry/Roughness data statistics

THIS PAGE INTENTIONALLY LEFT BLANK

VII. CONCLUSION

The current Navy doctrine for bottom roughness percentage is too ambiguous for analysis. It is very difficult to accurately determine the roughness percentage using model based off changes in depths. To calculate the bottom roughness percentage we proposed using the EM710 data to determine a reference level. The reference level will be used to determine the trend of the terrain. After removing the reference level from the 1-meter bathymetry, a threshold (2.5 m) is used to convert the data into bottom roughness percentage.

To find an accurate reference level we used a 200-meter window to subtract from the 1-meter bathymetry data, which gave us a change in height between the seafloor and the 1-meter terrain. Determining the correct window to use was the difficulty. The first attempt used a 100-meter window that did not reflect the actual trend of the seafloor. To calculate the number of roughness objects in an area, we needed to create a threshold. Various roughness objects were in close proximity with each and would blend in on the bathymetry data. To prevent the roughness from blending in with each other, a threshold was required. After testing various thresholds, we came to the conclusion that a 2.5-meter threshold gave us the best result. The final calculation showed that the test area contained 38% roughness. By applying the current Navy doctrine (greater than 15% = rough), the entire test area was considered rough terrain, even though a section of it was smooth. Instead of classifying the entire area rough, we broke up the test area into 25-meter grid boxes, showing the roughness for each grid, showing a true trend of the roughness.

Thresholds will need to be changed depending on the area surveying and will never be uniform. Roughness (craters, gullies, rocks) can blend in with each other making it difficult to accurately determine the roughness percentage; thresholds will have to be adjusted to prevent this. Propose using the gradient and mathematical morphology method to overcome ambiguity in the navy doctrine, to make it more objective and detailed. Using the new gradient method a more detailed and accurate description of the bottom roughness can be identified. The bottom roughness can be defined as smooth when the gradient is less than 0.05. Moderate bottom profile group can be found when

the gradient is between 0.05 and 0.15. The seafloor is considered to be rough when the gradient is greater than 0.15. Similarly for the mathematical morphology method, the seafloor is smooth when the roughness value is less than .09, moderate when it is between .09 and .24, and rough when it is greater than .24. Multibeam data provides quite accurate bathymetry and backscattering data for modeling roughness. The EM710 multibeam echo sounder can be an effective tool for mine warfare.

LIST OF REFERENCES

Bell, H. Jr., 1975: Statistical features of seafloor topography. *Deep-Sea Research*, Vol. 22, 883–892.

Berkson, J.M., and E. Matthews., 1984: Statistical characterization of seafloor roughness. *IEEE Journal of Oceanic Engineering*, Vol. 9, 48–51.

Brissette, M.B., 1997: The application of multibeam sonars in route survey. M.S. thesis, Graduate Academic Unit of Geodesy and Geomatics Engineering, The University of New Brunswick, 5 pp.

Caress, D., D. Chayes, and V. Schmidt, 2010: The MB-System cookbook. [Available online at http://www.ldeo.columbia.edu/res/pi/MB-System/mb-cookbook/].

Department of the Navy, 1996: NWP 3-15 Mine Warfare, 1996. DON, 50 pp.

Fisher, R., S. Perkins, and E. Wolfart, 2004: Image processing learning resources. [Available online at http://homepages.inf.ed.ac.uk/rbf/HIPR2/fourier.htm].

Fox, C.G., and C.E. Hayes., 1985: Quantitative methods for analyzing the roughness of the seafloor. *Reviews of Geophysics*, Vol. 23, 1–48.

Hammerstad, E., 2000: EM Technical Note: Backscattering and Seabed Image Reflectivity, 1–5.

Huang, M., L. Lee, C. Lin, S. Shyue, 2007: An Adaptive Filtering and Terrain Recovery Approach for Airborne LIDAR Data. *International Journal of Innovative Computing, Information, and Control*, July 2008, Vol. 4, No. 7, 2–12.

Kongsberg Maritime AS, cited 2012: The hydrographic product family brochure. [Available online at http://www.km.kongsberg.com/].

NOAA, 2011: DBDB-V Resolution Document, 2011. NOAA 23 pp.

——, 2011: NOAA Teachers at Sea EM710 Multibeam Echo Sounder. [Available online at http//:www.teacheratsea.wordpress.com/].

NSWC, 2007: Mine Countermeasures (MCM) Theory Primer, 2007. NSWC 139 pp.

Schwanghart, W., Kuhn, N. J., 2010: TopoToolbox: a set of Matlab functions for topographic analysis. Environmental Modeling & Software, 25, 1–11.

Teng, Y., 2011: Sector-specific beam pattern compensation for multi-sector and multi-swath multibeam sonars. M.E. thesis, Graduate Academic Unit of Geodesy and Geomatics Engineering, The University of New Brunswick, 90 pp.

USGS, 1998: The Bathymetry of Lake Tahoe, California-Nevada. [Available online at http://pubs.er.usgs.gov/#search:advance/page=1/page_size=100/query=98-509:0].

INITIAL DISTRIBUTION LIST

1. Defense Technical Information Center
   Ft. Belvoir, Virginia

2. Dudley Knox Library
   Naval Postgraduate School
   Monterey, California

3. RADM Jonathan White, USN
   Oceanographer and Navigator of the Navy
   Washington, DC

4. RADM Brian Brown
   Commander, Naval Meteorology and Oceanography Command
   Stennis Space Center, Mississippi

5. RADM Jerry Ellis (ret)
   Naval Postgraduate School
   Monterey, California

6. RADM Richard Williams (ret)
   Naval Postgraduate School
   Monterey, California

7. Mr. Robert Winokur
   Technical Director
   Oceanographer & Navigator of the Navy
   Washington, DC

8. Dr. William H. Burnett
   Technical Director
   Commander, Naval Meteorology and Oceanography Command
   Stennis Space Center, Mississippi

9. CAPT Greg Ulses
   Director USW
   Stennis Space Center, Mississippi

10. CAPT Paul Oosterling
    Commander, Naval Oceanographic Office
    Stennis Space Center, Mississippi

11. Mr. Thomas Cuff
Technical Director
Naval Oceanographic Office
Stennis Space Center, Mississippi

12. Dr. Richard Jeffries
Commander, Naval Meteorology and Oceanography Command
Stennis Space Center, Mississippi

13. Professor Mary L. Batteen
Naval Postgraduate School
Monterey, California

14. Professor Jeffrey Paduan
Naval Postgraduate School
Monterey, California

15. Professor Peter Chu
Naval Postgraduate School
Monterey, California

16. Mr. Ronald E. Betsch
MIW Program Manager
Stennis Space Center, Mississippi

17. Dr. James Rigney
Naval Oceanographic Office
Stennis Space Center, Mississippi

18. Dr. Daniel D. Sternlicht
Naval Surface Warfare Center

19. CDR William Sommer
Naval Postgraduate School
Monterey, California